University of Nevada, Reno

Geology of the Storm Gold-Silver Deposit Elko County, Nevada

A thesis submitted in partial fulfillment of the requirements for the degree of Master of Science in Geology

by

Richard B. Trotman

Dr. Tommy B. Thompson/Thesis Advisor

May, 2009

THE GRADUATE SCHOOL

We recommend that the thesis
Prepared under our supervision by

Richard B. Trotman

entitled

Geology of the Storm Gold-Silver Deposit
Elko County, Nevada

be accepted in partial fulfillment of the
requirements for the degree of

MASTER OF GEOLOGY

Tommy B. Thompson, Ph.D., Advisor

John Muntean, Ph.D., Committee Member

Alan Fuchs, Ph.D., Committee Member

Marsha H. Read, Ph.D., Associate Dean, Graduate School

May, 2009

Abstract

The Storm deposit is a high-grade gold deposit located near the convergence of the Carlin Trend and Northern Nevada Rift. Mineralization is primarily hosted within brecciated and ferroan-dolomite altered carbonates of the Silurian-Devonian Bootstrap Limestone Formation and to a lesser extent within Jurassic lamprophyre dikes. The deposit is a sedimentary rock-hosted gold deposit that contrasts with other Carlin-type deposits in that it is overprinted by younger low-sulfidation epithermal silver veins. Two successive mineralizing events are recognized and include a replacement style, gold-rich event characterized by decarbonatization, silicification, and sulfidation of carbonate-bearing strata with gold-bearing pyrite and native gold; and quartz-sulfide-selenide epithermal vein style silver mineralization with no visible, altered selvages.

The genesis of Storm deposit is complex and begins with pre-Mesozoic ferroan-dolomite alteration of carbonate rocks within the Dee Fault and along the contact between the Silurian-Devonian Bootstrap Limestone and the Devonian Popovich Formation. Emplacement of lamprophyre dikes and sulfidation of iron-bearing rocks during the Jurassic resulted in the creation of abundant pyrite that was the foci for subsequent gold-bearing hydrothermal fluids during the Eocene Carlin event. Gold is hosted by arsenic rich rims on pyrite with lesser amounts of hypogene native gold grains. Silicification temporally and spatially overlaps gold mineralization and is the dominant alteration type.

Silver-bearing, quartz-pyrite-selenide veinlets overprint gold-dominant Carlin mineralization and resemble those found in other epithermal vein deposits associated

with the Miocene Northern Nevada Rift. An apatite fission track date of 20.8 Ma from a dike within the main deposit supports a Miocene age for the silver values. Post-ore collapse brecciation as well as calcite ± barite precipitation during the Pliocene locally modified gold-bearing breccia bodies.

Table of Contents

List of Figures

Introduction

Sedimentary rock-hosted deposits of northeastern Nevada are substantial producers of gold and have been defined as a distinct deposit class in numerous publications during the past 40 years (Hausen and Kerr, 1968; Radtke et. al., 1972; Bagby and Berger, 1985; Arehart, 1996; Teal and Jackson, 1997; Hofstra and Cline, 2000; Thompson et. al., 2002; Cline et. al., 2005). While variations between individual deposits are common, all Carlin-type deposits share key geologic features. These include: (1) the presence of gold in fine-grained, disseminated, trace-element rich pyrite and/or marcasite, (2) replacement style mineralization in predominantly calcareous host-rocks, (3) structural and/or lithologic controls to orebody geometry, (4) geochemical association of gold with arsenic, antimony, thalium, and mercury, (5) high gold to silver ratios, (6) and hydrothermal alteration that includes decarbonatization, argillization, silicification, and sulfidation.

Storm is a deep, high-grade, refractory gold-silver deposit located within the Bootstrap mining district of Elko County, Nevada, and is the northern most known deposit on the Carlin trend. Storm is hosted in a sequence of Paleozoic passive margin sedimentary rocks exposed in a structural window of the Roberts Mountains thrust approximately 10 km northwest of the world class Betze-Post Carlin-type deposits and 10 km southeast of the Ivanhoe low-sulfidation epithermal gold-silver deposit (Fig. 1). The Storm mine is a collection of multi-stage, breccia-hosted orebodies (49'er, Discovery, and End Zones) occurring within a series of northwest trending high-angle normal faults 250 to 500 meters below the north high-wall of the Dee open cut gold mine.

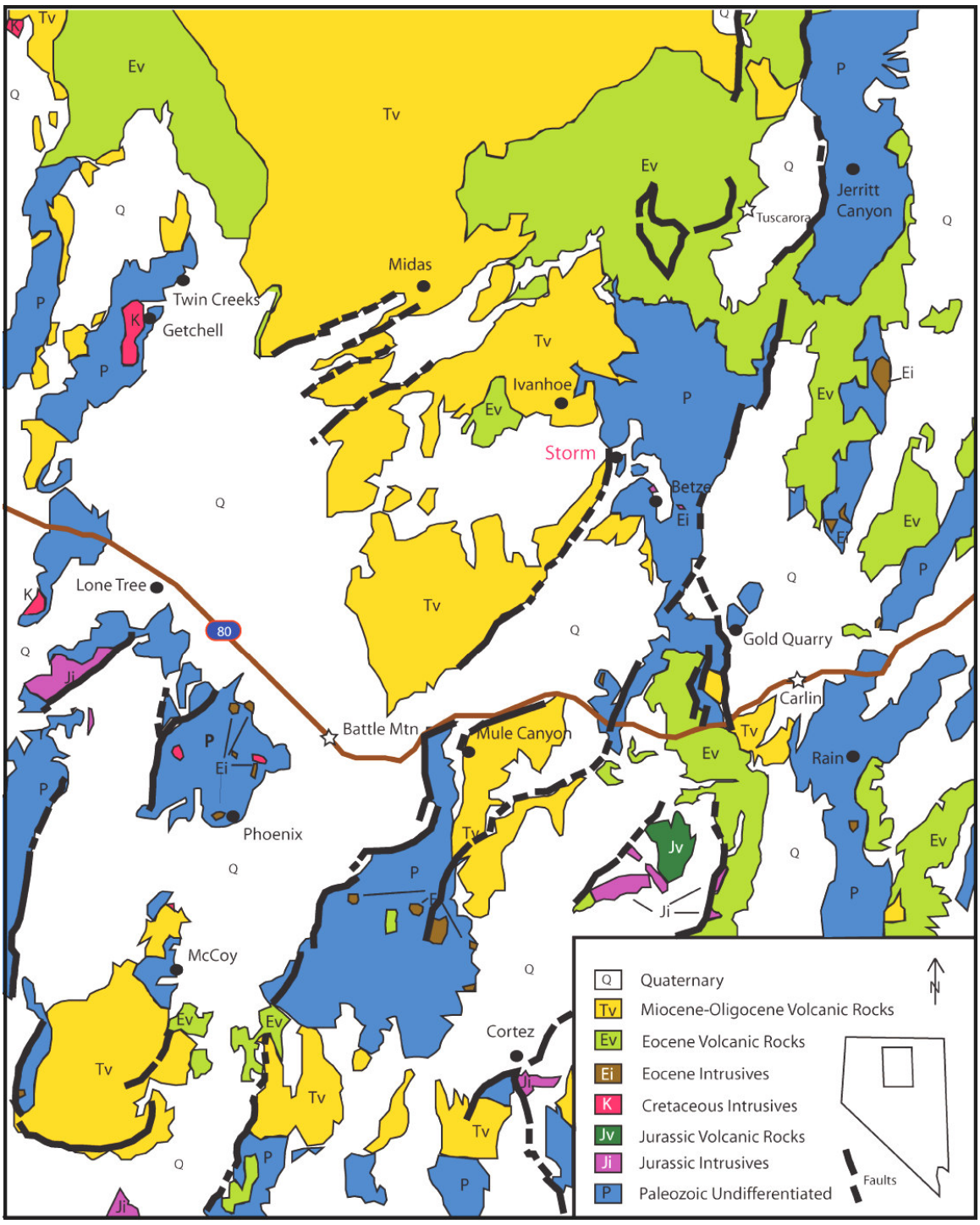

Figure 1. Regional geologic map of north-central Nevada showing major stratigraphic packages as well as the location of select ore deposits. Map was modified from Castor and others (2003).

Alteration is similar to other Carlin-type deposits, consisting of argillized, decarbonatized, dolomitized, silicified, and sulfidized assemblages. Mineralization typically occurs as silica-flooded, sulfide rich replacements of ferroan dolomite-altered limestone breccias that occur at the tectonic contact of the Ordovician-Silurian Vininni Formation and underlying Devonian-Silurian Bootstrap Limestone.

The scope of this paper is to present a detailed geologic overview of the Storm deposit, which is a high-grade Carlin-type gold deposit that also contains significant silver and has lower gold to silver ratios than typical Carlin-type deposits. Storm potentially represents a variation from the norm, and, thus, presents an opportunity to increase our understanding of Carlin-type deposits.

District History

The Storm deposit is part of the Bootstrap mining district, which is comprised of the Bootstrap, Tara, Capstone, and Dee mines, and is the northern-most known cluster of Carlin-type gold deposits on the Carlin trend (Fig. 2). Initial interest in the district was focused on the production of antimony ores from the Bootstrap mine during the 1910's. Gold potential was later realized during the 1950's and most of the early production came from highly altered and mineralized porphyry dikes at Bootstrap (Nuckolls, 1985; Evans, 2000). The identification of low-grade disseminated ores led to further development of the Bootstrap mine as well as the discoveries at Tara, Capstone, and Dee.

The Dee mine was discovered in 1981 by Cordex Exploration Company and put into production by the Dee Mining Company and Rayrock Mines Inc. in 1984. The Dee mine produced approximately 682,000 ounces of gold and 400,000 ounces of silver from 80 million tons of oxide heap-leachable ore (Cook et al., 2002; Dobak et al., 2002). Although silver recoveries were low, average silver to gold ratios at Dee averaged 3 to 1 (Bergwall, 1991). Mining operations ceased in 2000, at which time reclamation of the site and facilities began.

Storm is accessed from a decline near the bottom of the Dee open pit (Fig. 3). The deposit is a collection of low tonnage, high-grade, refractory orebodies that, to date, hold pre-mining measured and indicated reserves totaling 861,000 tons grading 0.447 ounces per ton gold. An additional 431,000 tons grading 0.408 ounces per ton are held as an inferred resource (personal communication, Arbonies, 2006). While

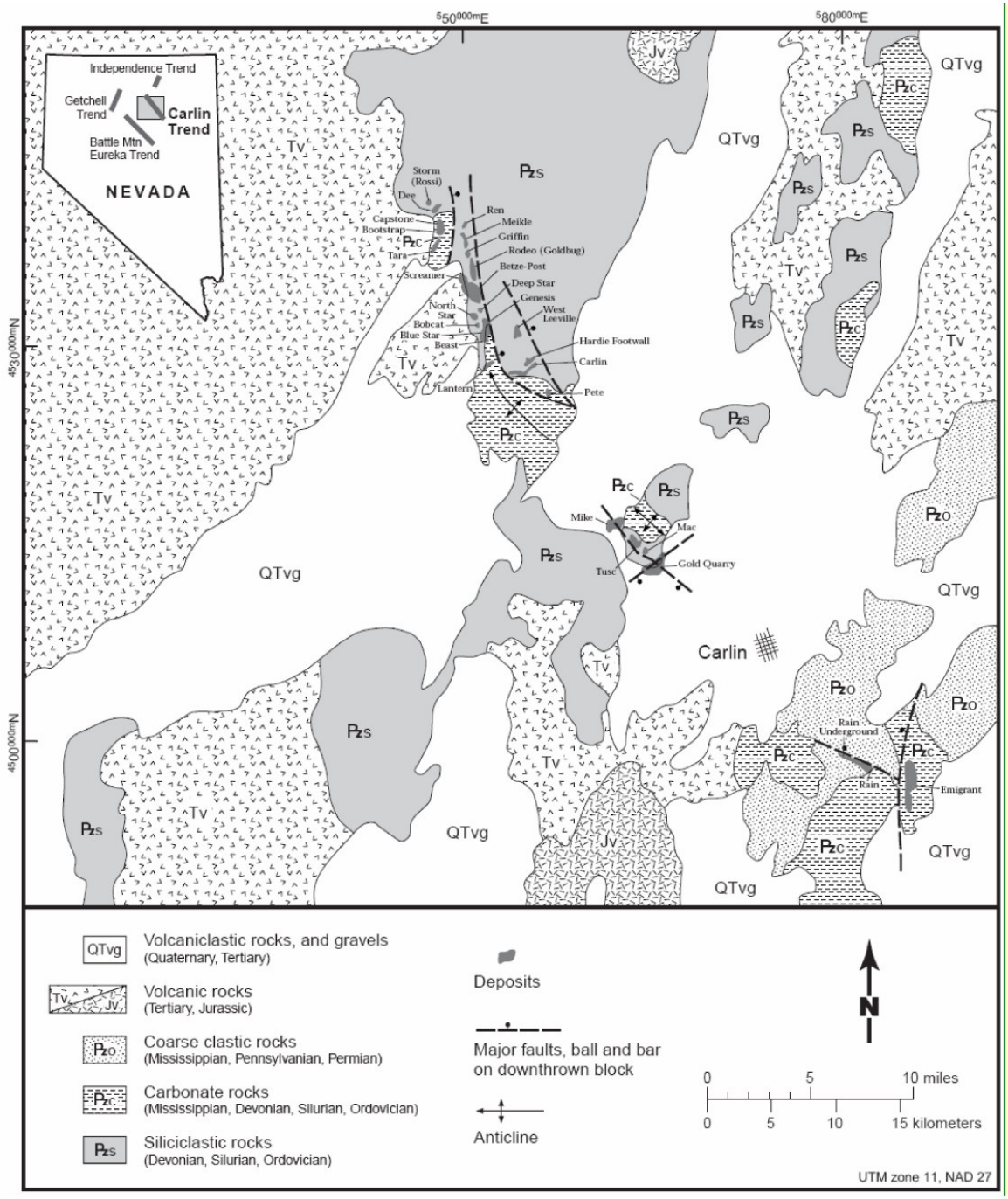

Figure 2. Geology of the Carlin Trend, Northern Nevada. Storm is the northern most mine located along the trend. Figure taken from Teal and Jackson (2002).

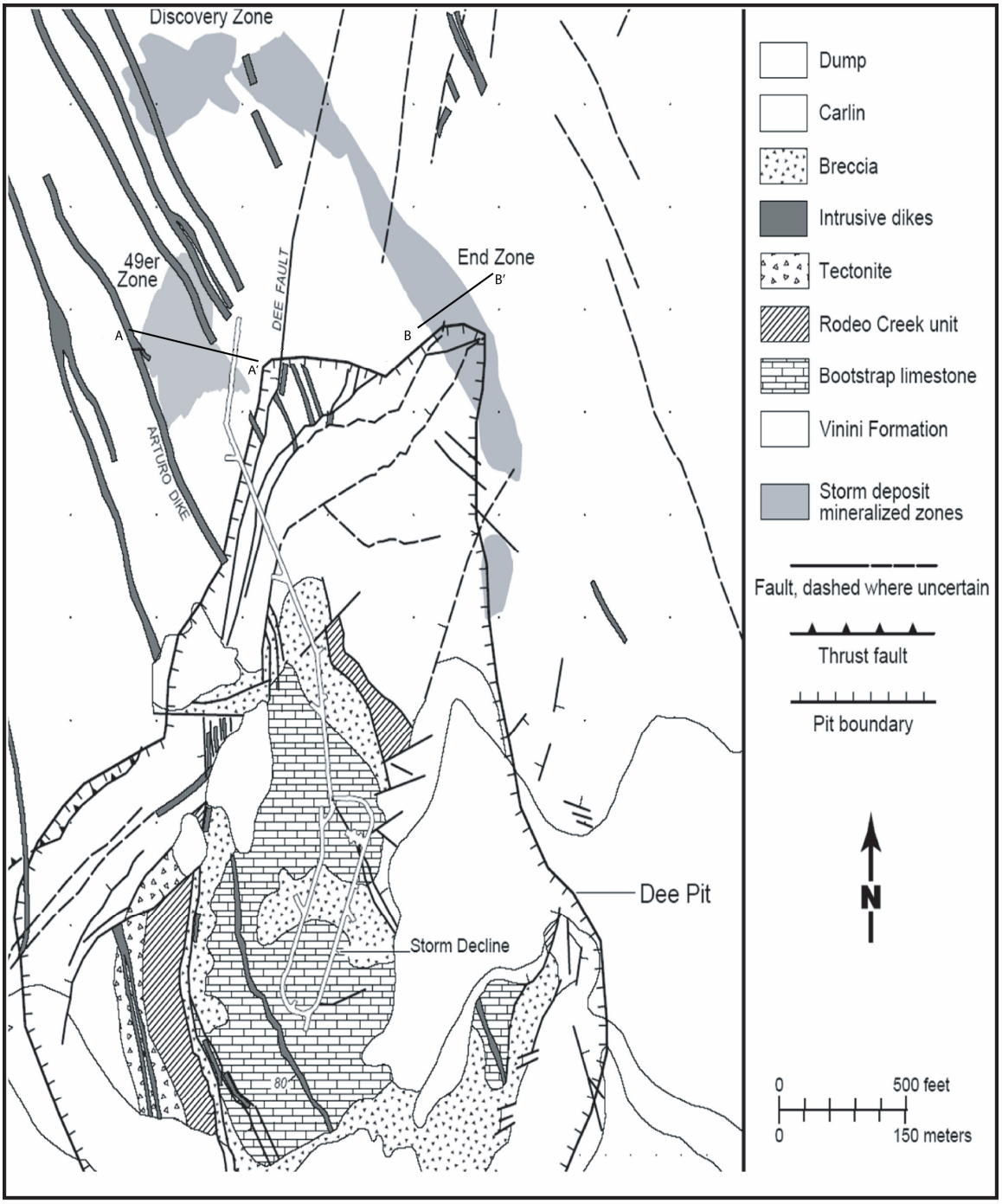

Figure 3. Shows the outline of the Dee open pit as well as the outline of the main mineralized zones at Storm. Taken from Dobak and others (2002).

the exact silver resource has not been calculated, average silver to gold ratios (4:1) at Storm indicate the presence of approximately 2.2 million ounces of silver. Historical production plus remaining reserves/resources in the Bootstrap district total 3.2 million ounces of gold (Teal and Jackson, 1997).

Methods

Approximately 3,000 meters of diamond drill core (1" = 20' scale) were logged during the summer of 2005 with an emphasis on lithology, alteration, mineralogy, structure, and physical characteristics of breccia bodies. Gold assays and trace element geochemical results were taken from Barrick Gold Exploration Inc.'s database for the Storm deposit. All drill-hole samples were taken from split HQ-diameter core intervals that had recovery of greater than 50 percent.

The Electron Microanalysis and Imaging Laboratory at the University of Nevada, Las Vegas provided the use of a JEOL-8900 Electron Probe Microanalyzer to determine the composition of pyrite and various sulfosalts minerals. Quantitative analyses have detection limits of 0.01% (100 gram/ton) for each element analyzed. Cathodoluminescence images were taken with an Oxford/Gatan Mini-CL Cathodoluminescence Detector which was mounted within the JEOL-8900.

Age dating using apatite fission track analysis was performed on one sample of altered and mineralized lamprophyre dike material from the 49'er Zone by Geotrack International Pty Ltd.

Microthermometric measurements were conducted at the University of Nevada, Reno on a FLUID Inc. heating-freezing stage mounted to an Olympus BX51 transmitted light microscope and are accurate to within $\pm$ 0.1^{o}C (heating) and $\pm$ 1.0^{o}C (freezing). Homogenization temperatures of individual inclusions can be found in Appendix I.

Regional Geology

Precambrian rifting along the western margin of the North American craton resulted in a westward facing, passive continental margin. A progressively thickening wedge of sedimentary rocks accumulated through the early Phanerozoic until at least the late Devonian. An eastern miogeoclinal assemblage (Fig. 4) consisting primarily of shallow water shelf and platform carbonates progressively grades into a western eugeoclinal assemblage consisting of clastic siliceous sediments, deep water carbonates, and chert dominated sequences (Stewart, 1980).

Passive margin sedimentation ceased during the late Devonian to early Carboniferous and was replaced by a compressional tectonic regime during the Antler Orogeny. Large-scale faulting resulted in western eugeoclinal clastic rocks being thrust over eastern miogeoclinal carbonate facies assemblages (Roberts et al., 1960). This fault or system of faults – known as the Roberts Mountain thrust - extends from Central Idaho to Southern Nevada and is defined by a low-angle thrust faults that place allochthonous "upper plate" siliceous rocks over autochthonous "lower plate" carbonate facies rocks.

Eastward subduction of the Farallon plate beneath the western margin of the North American continent during the Triassic to Oligocene resulted in the formation of the Elko and Eureka fold and thrust belts in Eastern Nevada (Thorman et al., 1992). A dominant set of broad north-northwest trending folds, roughly parallel to the trace of the Carlin trend, were formed during this east-northeast directed

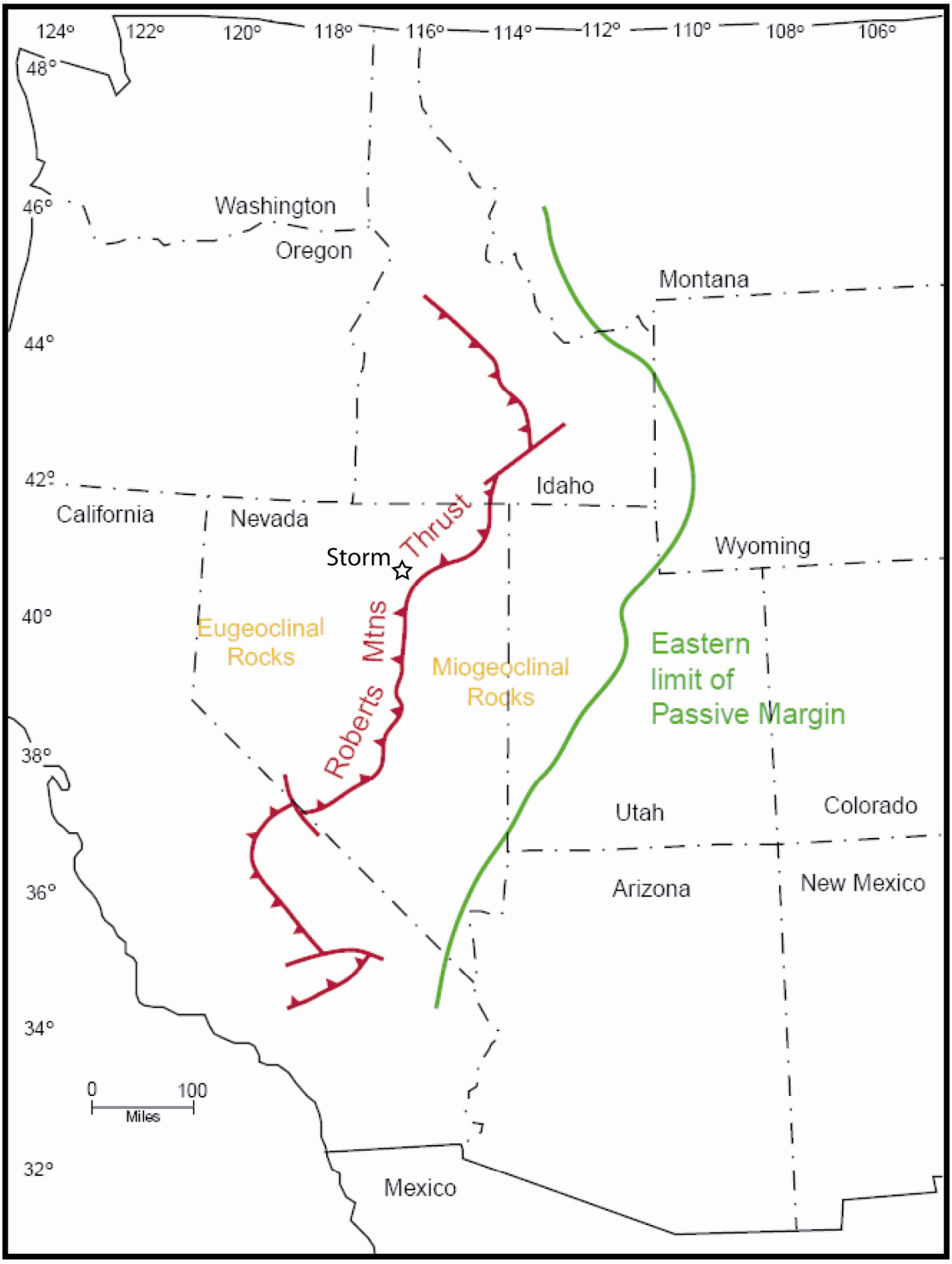

Figure 4. Shows the location of passive margin sedimentation on the western edge of the North American craton during the Paleozoic. Also shown is the approximate trace of the Roberts Mtns Thrust. Modified from Furley (2001).

compressional regime (Roberts, 1960). Many of these folds commonly host Carlin-type gold deposits.

Emplacement of Mesozoic stocks and associated dikes occurred along preexisting fault systems flanking the north-northwest trending folds. The Goldstrike stock is the largest in the northern Carlin trend and has been dated at ~158 Ma (Arehart et al., 1992). The emplacement of these intrusive bodies further enhanced fracture systems peripheral to the stocks and dikes that later acted as important ore fluid conduits (Cline et al., 2005).

The progressive rollback of the Farallon plate beneath North America during the Oligocene-Miocene resulted in widespread magmatism that swept south from northern Nevada beginning ~42 Ma (Cline et al., 2005). Numerous Tertiary sills and dikes have been documented within the Carlin trend (Emsbo et al., 1996; Ressel et al., 2000). During the mid-Tertiary, a change from a compressional to an extensional tectonic regime resulted in large scale extension leading to the creation of the Basin and Range province, the development of metamorphic core complexes, and widespread volcanic activity in Nevada (Cline et al., 2005).

Local Geology

The stratigraphy at Storm can be divided into four major packages: an autochthonous sequence of Lower Paleozoic shelf and slope-facies carbonate rocks structurally overlain by an allochthonous sequence of Lower Paleozoic deep-water siliceous rocks that are in turn capped by Tertiary volcaniclastics (Teal and Jackson, 1997). Two suites of igneous dikes, Jurassic biotite-lamprophyres and Eocene basaltic andesites, cut both Paleozoic sedimentary sequences (Dobak et al., 2002). The following stratigraphic units are described using informal naming conventions used widely by Barrick Gold Inc. geologists. Figure 5 is a stratigraphic column for the Storm property.

Miocene Carlin Formation: The Miocene Carlin Formation is a sequence of tuffaceous lacustrine sediments, air-fall tuffs, and gravels that unconformably overlie western-assemblage upper-plate rocks in the Storm area. Surface outcrops are seen primarily to the south, west, and east of the Dee open pit, with minor occurrences of channel fill material to the north. The total thickness of the Carlin Formation on the Storm property is generally less than 120 meters, although it is known to be greater than 300 meters thick to the southeast of Storm, on the Goldstrike property (C. Weakly, personal communication, 2006).

Three distinct units of the Carlin Formation have been observed in the Storm area. The uppermost unit is unconsolidated to semi-consolidated red-brown silt to sand sized lacustrian sediments that usually contain a significant amount of ashy material. The middle unit is a series of variably consolidated quartz-sanidine-orthoclase feldspar

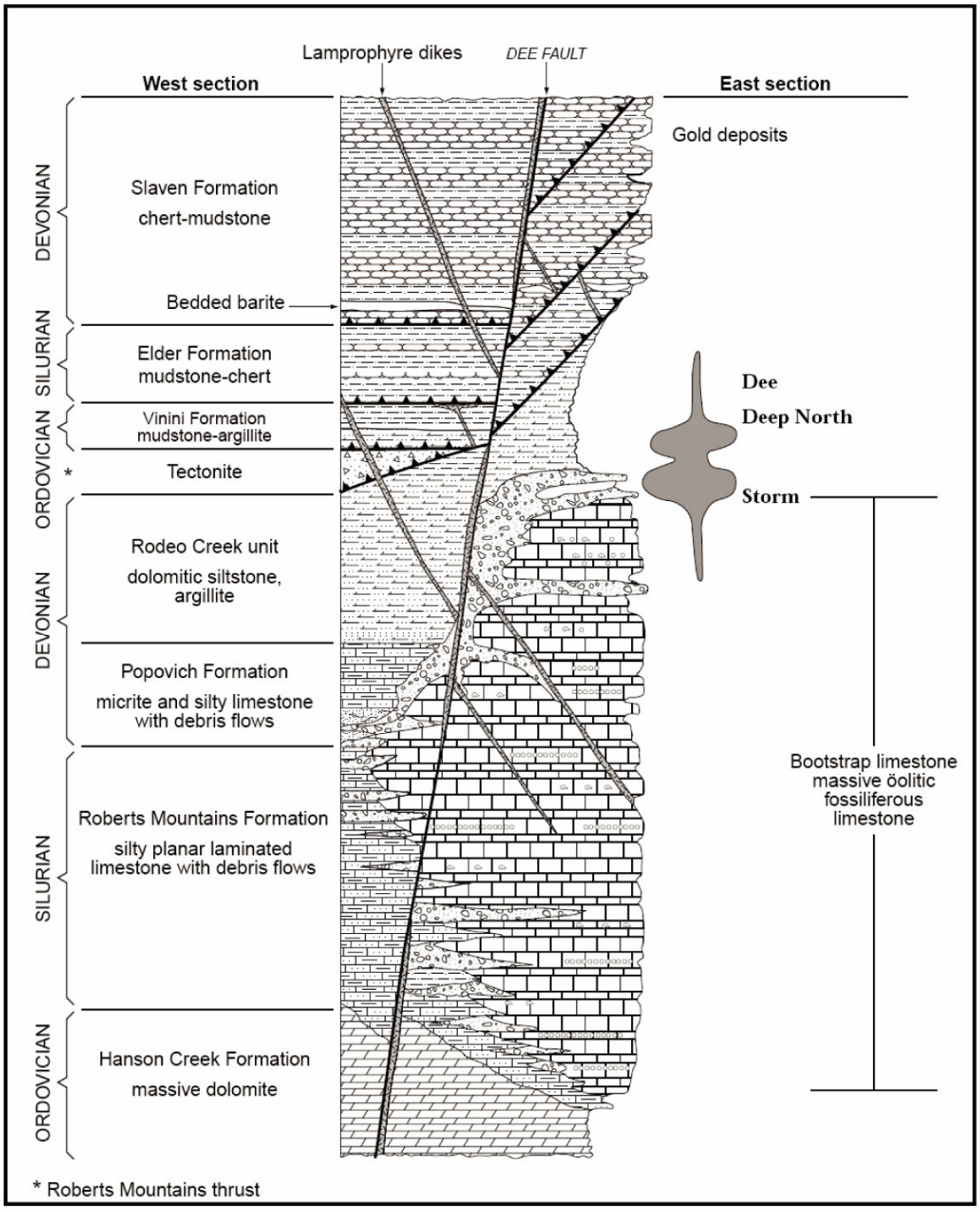

Figure 5. Stratigraphic column for the Storm property. Taken from Dobak and others (2002).

bearing ash-fall tuffs that have Ar^{40}/Ar^{39} ages ranging from 14.3 to 15.3 Ma (Fleck et al., 1998). The basal unit consists of clast- to matrix-supported gravels containing weathered fragments of siliceous Paleozoic cherts, silicified mudstones/siltstones, jasperoid, and local igneous dike fragments. Matrix material can locally contain silts and/or ash from the overlying units. Light green to yellow halloysite clay zones commonly form immediately above the basal gravel units, within or near the margins of the ash-fall units, or along large structures (C. Weakly, personal communication, 2006).

Devonian Slaven Formation: The Devonian Slaven Formation is seen locally in the Storm area and is recognized as an undifferentiated package of thin-bedded green, grey, black, and brown cherts with local bedded barite and green mudstone. The Slaven Formation is invariably sheared, folded, and tectonically imbricated.

Silurian Elder Formation: The Silurian Elder Formation consists of three units ranging in thickness from 10 to greater than 100 meters. The upper unit is comprised of interbedded grey, white, and black siliceous mudstone and cherts. The middle unit is an olive-buff to red lithic siltstone containing 0.1 mm translucent mica flakes. This can be interbedded with grey to black mudstones and/or chert. The basal unit, the Cherry Springs Chert member, is a thin to thick bedded dark green chert that locally contains 1-5mm spherical vugs. The Elder Formation has been observed, in outcrop and drill core, to the North and East of the Dee open pit.

Ordovician Vinini Formation: The Ordovician Vinini Formation is a sequence of interbedded mudstones, siltstones, cherts, silicified mudstones, and jasperoid. In the Storm region, the Vinini Formation is strongly sheared, structurally imbricated, and has a fold fabric that plunges gently to the north-northwest. The Vinini Formation structurally overlies the lower-plate assemblage of carbonate-dominant strata and can achieve a thickness of over 700 meters. Where visible, this contact is a sharp, low-angle thrust. Dense quartz vein stockworks occur locally and routinely contain trace amounts of gold and silver along with anomalous pathfinder element geochemistry (As, Sb, Hg, etc). The Vinini Formation hosts several small, structurally-controlled and sheeted-vein hosted gold deposits along the Northern Carlin trend such as Capstone, Big Six, Fence, and Antimony Hill (Teal and Jackson, 1997).

The Upper Vinini is divided into three distinct subunits. The uppermost subunit is a light-grey limestone that is typically altered to a butterscotch-brown colored jasperoid and is between 0 and 7 meters thick. The middle subunit commonly referred to as the BS chert by Barrick Goldstrike geologists, is a 15-20 meter thick sequence of black to dark brown thin-bedded cherts with local interbedded mudstones and/or mudstone partings. Below this unit is a 10-15 meter thick sequence of light grey to pink thin to thick bedded cherts that is underlain by a 100-150 meter section of light grey to black thin bedded siltstones, mudstones, and cherts.

The Lower Vinini is typically a 400 to 550 meter thick sequence of light to dark grey mudstones, siltstones, and cherts that exhibit strong folding and shear foliations with local dense quartz vein stockworks. Due to the strong structural deformation that occurs within the Lower Vinini, a preserved section has yet to be described in the Storm region.

Therefore, the following descriptions may not be presented in a correct stratigraphic context. The uppermost observed unit is a grey thin bedded mudstone, siltstone, and silty-mudstone with local grey chert lenses/laminations. Below this unit is a sequence of light grey mudstone with thick beds of black chert and local siliceous mudstone. This unit locally contains thin planar laminated dolomitic siltstones with alternating dark and light colored laminations. The basal unit is typically a thick section (>100 meter) of black and grey flaser laminated mudstones and siliceous mudstones with local black chert lenses/laminations (Fig. 6). The base of the Lower Vinini, if present, is in fault contact (Roberts Mtns Thrust) with "lower-plate" calcareous rocks.

Devonian Rodeo Creek Formation: The Rodeo Creek Formation is found throughout the Northern Carlin trend and hosts gold mineralization in the upper portions of the Betze-Post, Genesis, Gold Quarry, and Blue Star deposits (Teal and Jackson, 1997; Bettles, 2002; Jory, 2002).

The upper unit of the Rodeo Creek Formation, the upper argillite, is a 30 to 60 meter thick unit of thin planar-bedded silicified black mudstones with minor mudstone, siltstone, and chert. The middle unit, the Bazza Sands, is a sequence of thin to medium bedded dark and light grey interlaminated siltstone, calcareous siltstone, and muddy siltstone. The Bazza Sands are locally decarbonatized, silicified, and host the bulk of the gold mineralization found within the Rodeo Creek Formation. The basal unit of the Rodeo Creek Formation, the Lower Argillite, unconformably overlies the Devonian Popovich Formation and consists of black thin-bedded silicified mudstones with lesser

Figure 6. Laminated mudstones and silicified mudstones of the Lower Vinini Formation. Core is HQ; box represents 3.05m (10ft).

amounts of interbedded siltstone, mudstone, and local chert. While the Rodeo Creek Formation locally exceeds 300 meters in thickness in the Goldstrike region, it is less than 200 meters thick at Storm. North of Storm, near Rossi, it thickens too nearly 750 meters. At Storm, only the lower unit of the Rodeo Creek Formation has been observed to date (Fig. 7).

Devonian Popovich Formation: The Popovich Formation is present throughout the Carlin trend and hosts the bulk of Carlin-type gold mineralization in Betze-Post, Screamer, Rodeo, and Deep Post (Bettles, 2002; Teal and Jackson, 2002). The Popovich Formation is a package of dominantly calcareous mudstones, muddy limestones, debris flows and turbidite sequences that consist of four main subunits that achieve a maximum combined thickness of 400 meters. Ettner (1989) as well as Armstrong et al. (1997) have interpreted the Popovich Formation as being slope to toe-of-slope facies and suggest it was deposited over the Bootstrap Limestone shallow slope facies as water levels progressively deepened. On the Storm property, a complete section of Popovich Formation occurs west of the Dee Fault while only the uppermost muddy unit is present on the eastern side (Dobak et al., 2002).

Silurian-Devonian Bootstrap Formation: The Bootstrap Formation consists of massive, sparry, and oolitic to peloidal limestone (Fig. 8) that ranges in thickness from 20

Figure 7. Silicified mudstones of the Rodeo Creek Formation. Core is HQ; box represents 3.05m (10ft).

Figure 8. Representative interval of the Bootstrap Limestone from the Storm deposit. Core is HQ; box represents 3.05m (10ft).

to over 600 meters throughout the northern Carlin trend. Limestones are locally fossiliferous, containing corals, bryozoans, brachiopods, and mollusks (Evans, 2000). Calcite veins up to several meters thick are found throughout the section, as are dark-grey to black stylolites. The Bootstrap Formation is time equivalent to the Roberts Mountains Formations (SDrm) (Griffin, 2000) and commonly interfingers with the SDrm on the western side of the Storm property. This entire package is believed to have been deposited in a largely open platform margin to shallow slope depositional environment (Ettner, 1989; Armstrong et al., 1997). The Bootstrap Limestone hosts the bulk of gold mineralization at Storm and is an important host-rock for the Meikle, Griffin, Banshee, and Dee deposits.

Silurian-Devonian Roberts Mountains Formation: The Roberts Mountains Formation occurs conformably below the Popovich Formation and is time equivalent to Bootstrap Limestone. In the Northern Carlin trend, the Roberts Mountains Formation primarily consists of light to dark grey bedded to laminated limestones with interbedded debris flows. Two mappable units have been identified, an upper transitional unit that contains wispy bedded muddy limestone interbedded with significant massive limestone debris flows and a lower unit of dark to light grey planar banded limestone to silty limestone. In the Storm area, the Roberts Mountains Formation crops out southwest of the Dee mine and occurs in drill core throughout section west of the Dee Fault.

Hanson Creek Formation: The Hanson Creek Formation is the oldest known formation in the Storm area and is characterized as thick to thin bedded, white to pink

colored sandy dolostone. To date, the Hanson Creek Formation has only been reported in a hand-full of deep drill holes located west of the Dee Fault (Dobak et al., 2002).

Jurassic Lamprophyres: The most common intrusive rock in the Storm area is a series of porphyritic Jurassic hornblende-pyroxene-biotite dikes. The least altered samples are light greenish-grey and contain abundant 0.1 to 0.5 mm lathy hornblende, 0.2 to 1.5 mm green pyroxene, and 0.1 to 1.0 mm biotite phenocrysts in a fine-grained groundmass. Rare earth element concentrations suggest a basaltic-andesite composition for this variety of lamprophyre dike found at Storm. An $^{40}Ar/^{39}Ar$ age date of 162 Ma has been reported by Dobak et al. (2002) from a lamprophyre dike within the Dee open pit.

The Jurassic lamprophyres typically form as high-angle dikes and dike swarms that can locally occupy normal faults such as the Dee fault. Dikes form sharp contacts with surrounding stratigraphy and are locally internally brecciated. Cross-cutting relationships show that emplacement of lamprophyre occurred after the onset of high-angle faulting and early breccia formation. Reactivation of large structures such as the Dee fault resulted in tectonic brecciation of dikes crossing such zones.

Eocene Basalts: A series of basaltic dikes are locally found within the Dee fault within the Dee open pit and have been reported by Dobak et al. (2002) within the same fault system at Storm. These dikes are basaltic in composition, containing large pyroxene, olivine, and plagioclase phenocrysts in a fine-grained groundmass. Ressel (2006) reported a whole rock $^{40}Ar/^{39}Ar$ date of 37.57 ± 0.34 Ma from a basalt sample

collected from the Dee open pit. Basaltic dikes were not observed during this study, although it is possible that highly altered basaltic dike fragments may be present within mineralized breccias.

Structure

The majority of gold and silver mineralization at Storm is strongly influenced by structural controls, primarily highly fractured and brecciated zones within or peripheral to fault systems or fault intersections. The largest of these mineralized zones generally occur within thick (>30m) breccia zones located where high-angle normal faults intersect the upper contact of the Bootstrap Limestone Formation.

The structural evolution of the Northern Carlin trend has been thoroughly discussed by many authors (Roberts, 1960; Leonardson and Rahn, 1996). The following section describes the geometric and kinematic characteristics of the structures found on the Storm property.

Low-Angle Faults: The oldest documented structural features on the Storm property are low-angle (<30^{o}) structures associated with the Roberts Mountains thrust (Fig. 9). Strongly sheared and locally flaser laminated mudstones of the Vinini Formation commonly appear foliated and can have thin gouge zones and/or crush breccias along individual shear planes. Thrusting along shear planes resulted in duplexing of upper plate strata, making it hard to estimate an original depositional thickness. Lower plate carbonate rocks are normally much less affected by low angle structures. Low-angle structures are typically cut by high-angle faults. Low-angle normal offsets documented within several dikes on the Storm property may indicate reactivation during later stages of deformation.

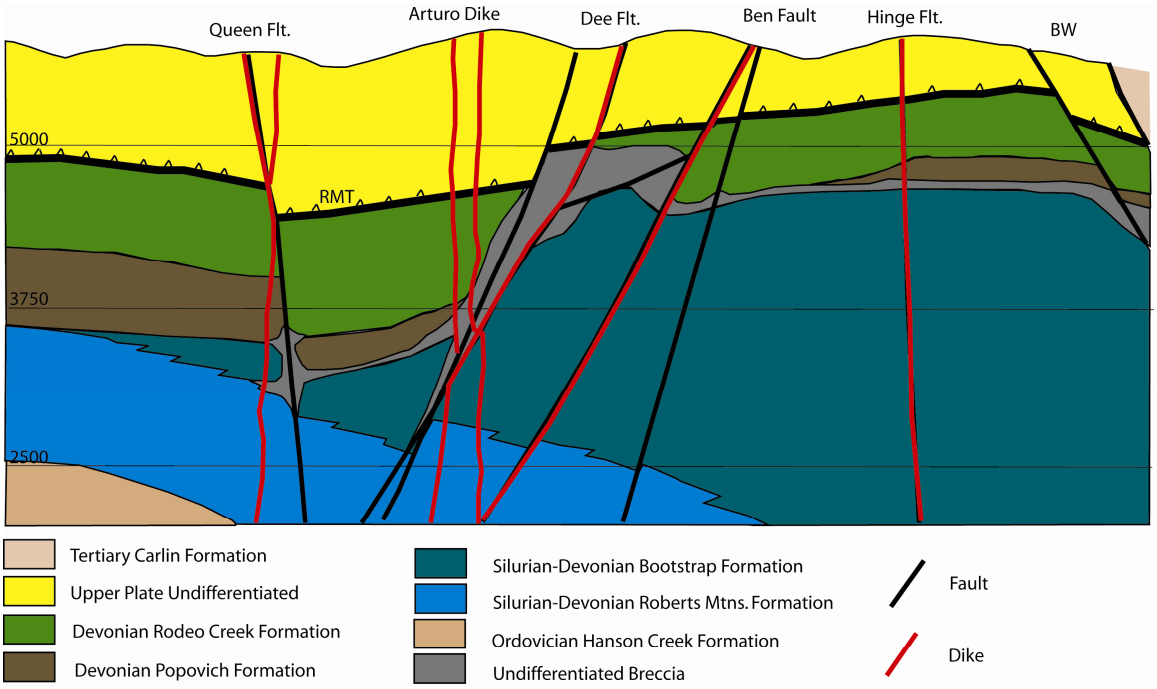

Figure 9. Type section at 292000N showing the local stratigraphy at Storm as well as major faults and breccia zones. Units are the same as those described on Figure 2.

High-Angle Faults: Like most of the northern Carlin trend, high-angle faults on the Storm property are the most important ore-fluid conduits and hence the primary control on mineralization. Four sets of faults with apparent normal offset have been documented and are listed in order of decreasing importance as ore hosts: north-south, northeast, north-northwest, and northwest. Most of the mineralized high-angle faults in the northern Carlin trend, such as the Post and Bootstrap faults, are oriented roughly parallel to the trace of the Carlin trend (northwest). At Storm, the Dee fault system is the major ore-controlling structure and is oriented north-south through the Dee open pit and shifts to N5^{o}E, north of the Storm deposits.

The Dee fault has between 125 and 600 meters of normal offset. Many of the mineralized structures at Storm such as the Ben, End Zone, Queen, and BW series faults have less than 30 meters of displacement (Fig. 9). The intersections of high angle faults are by far the most important ore controls at Storm, especially where they occur near key stratigraphic contacts such as the Bootstrap-Popovich Formation boundary.

Breccias

Gold and silver mineralization at the Storm deposit is almost exclusively associated with a complex set of multistage breccia bodies. Two distinct breccia types have been documented: 1) tectonic breccias, including crackle breccias, created due to the crushing, shattering, and shearing of rocks during the movement of large structural features (i.e., Dee, End Zone, and Ben faults), and 2) hydrothermal dissolution/collapse breccias related to rock dissolution and volumetric reduction of carbonate-rich units. Overprinting stages of breccia and hydrothermal alteration are quite common within breccia bodies and commonly convolute cross-cutting relationships and the overall geometry of individual breccia types.

Tectonic Breccias: The most voluminous and perhaps important breccia type at Storm is tectonic breccia. Tectonic breccia typically exhibits high-angle, tabular, sheet-like geometries and locally exceed one kilometer in strike length and are the primary control on the flow of hydrothermal fluids. Breccia thicknesses average 5 to 15 meters, except at structural intersections and at the upper contact of the Bootstrap Limestone, where they can be up to an order of magnitude larger in scale.

Footwall to these fault zones are highly fractured hydrothermal crackle and mosaic breccias that are comprised entirely of limestone protolith fragments. These breccias are characterized by dilated fractures having matching walls and where no fragment rotation has occurred. Fragments account for greater than 80% of the breccia mass, and matrix material is either ground up rock or more commonly massive quartz

flooding (Fig. 10). Crackle breccias can be up to 10 meters thick and locally form a cap or apron above unaltered massive limestone of the Bootstrap Formation. Low grade gold and silver mineralization, locally up to 6 gram/ton, is present within zones of intense crackle brecciation.

Crackle breccias usually grade upwards into more intensely deformed cataclastic rocks that locally exhibit weak to moderately developed tectonic fabrics. These tectonic breccias can be either matrix- or fragment-supported but typically contain at least 30% matrix material. Unaltered matrix is comprised of fine grained limestone and/or mud rock flour and is only locally preserved. The bulk of the matrix material has been completely replaced by quartz ± carbon ± sulfides. Fragments are angular to sub-angular, average 0.5cm to 20cm, and are invariably altered to some degree.

The tectonic breccias at Storm have been sub-classified by Barrick geologists based on dominant lithology (e.g. dolomite breccia or mudstone breccia) in order to more accurately map the multi-stage breccia bodies. Dolomite breccias contain greater than 75% limestone protolith fragments and are much more favorably mineralized than mudstone breccias, which contain greater than 25% mudstone, chert, and/or siliceous mudstone fragments. Within the Dee fault, dolomite breccias typically grade upward into mudstone breccias. Discontinuous zones of rock gouge are found locally within tectonic breccias and record periods of intense deformation related to large-scale fault displacements. One zone of continuous fault gouge has been identified within the 49'er Zone and forms a discreet 10 to 15 cm thick zone at the upper margin of the Dee fault.

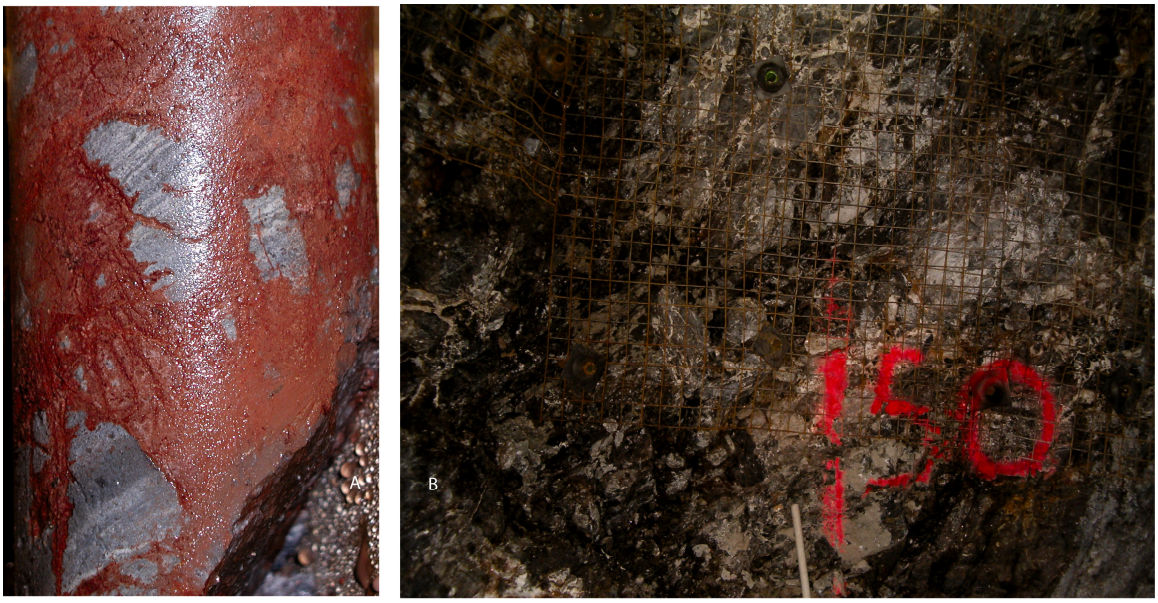

Figure 10. Examples of tectonic breccias at Storm. A. core sample (2.5″) showing igneous dike fragments in oxidized quartz-rock flower matrix. B. Photograph from the 49′er ore zone cross-cut. Shows tectonic breccia (brown matrix) containing large blocks of silicified collapse breccia (white matrix).

Loose constraints on the timing of tectonic brecciation are based on cross-cutting alteration and structural relationships. While there may have been multiple movements along the Dee fault since mineralization, the main stage of brecciation must have occurred after emplacement of the Roberts Mountains allochthon and the onset of dolomite alteration.

Hydrothermal Dissolution/Collapse Breccias: Two stages of collapse brecciation are recognized at Storm. The first stage occurred prior to the emplacement of Jurassic dikes and resulted from the conversion of pure limestone to hydrothermal dolomite. Volume reduction of the supporting carbonate column due to dolomitization resulted in local collapse breccias that form irregular shaped bodies. The preferential flow of

hydrothermal fluids along major structures centered these collapse breccias within and proximal to pre-existing tectonic breccias. Similarly, the same fluids locally spread out laterally from the fault zones where they encountered favorable stratigraphic contacts, such as the Bootstrap-Roberts Mountains and Bootstrap-Popovich formations contacts.

The second stage of collapse brecciation was a post-mineral event. The fluids responsible for the dissolution and collapse of carbonate material utilized pre-existing structural and stratigraphic contacts. These breccias locally modify ore material and are commonly cemented by massive white calcite with local barite crystallization. Similar dissolution/collapse breccias documented at the nearby Meikle deposit have been dated at approximately 2 Ma (Emsbo and Hofstra, 2003). The possibility exists that these breccias formed during the same hydrothermal event.

Collapse geometries from both breccia events are generally pseudo-circular in plan view and range in diameter from a few meters to 10's of meters across. In cross-section, collapse breccias form bulbous or swollen zones that are typically thickest near the middle of the pile, ranging up to 20 meters in vertical extent. Fragments are comparatively larger than those found within tectonic breccias. Boulder sized fragments of limestone are not uncommon in stratigraphically controlled collapse breccias, whereas collapse within pre-existing tectonic breccias typically results in further reduction of fragment size. The majority of collapse breccias at Storm are fragment supported with

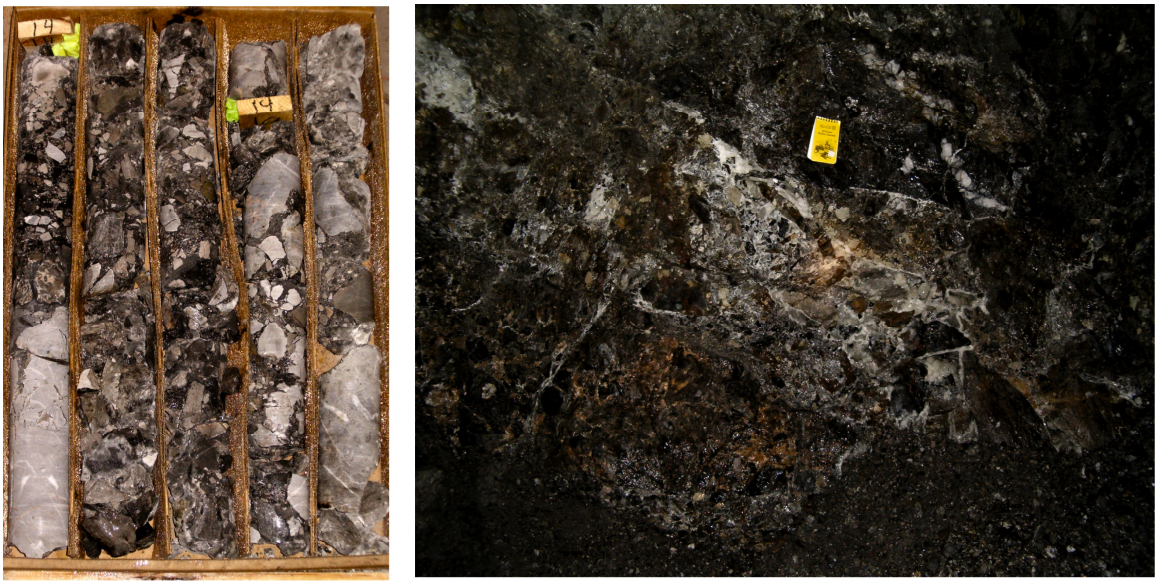

Figure 11. Examples of collapse breccias. A. Post-ore collapse breccia with little post-mineral alteration. Note the pyritized fragments (grey to black colored). B. Silicified collapse breccia from the End Zone drift.

fine-grained limey matrices that are typically replaced by later stages of either massive quartz or calcite flooding (Fig. 11). Post-mineral collapse breccias are locally cemented by massive white calcite and may contain fragments of ore material. Calcite and barite crystals have been documented within void spaces.

Alteration

While the hydrothermal alteration associated with Carlin-type ore deposits has been described by many authors (e.g., Bakken and Einaudi, 1986; Arehart et al., 1992; Kuehn and Rose, 1992; Arehart, 1996; Hofstra and Cline, 2000; Cline et al., 2005), a model based on temporal and/or spatial zoning relationships has yet to be produced that can adequately use alteration as a direct vectoring tool for gold mineralization. Despite this, most Carlin-type deposits do show a general alteration assemblage that includes decarbonatization of primary carbonate host rocks, variable intensity of silicification in the form of jasperoids, argillization of primary igneous bodies, and sulfidation of Fe-bearing minerals resulting in gold deposition.

Similar to the Meikle deposit, the main ore zones at Storm are hosted primarily within dolomitized and decarbonatized Bootstrap Limestone Formation and limestone breccia bodies (Evans, 2000). A general progression of alteration is clearly visible at Storm that suggests dolomitization of limestone was followed by an early stage of silica replacement (creating jasperoid) and carbonate removal prior to the main Carlin gold event. At least two later silicification events, which include the deposition of silver-rich epithermal vein style mineralization, were then followed by late stage argillization, calcite ± barite deposition, and oxidation.

Dolomitization: Dolomite alteration exhibits both structural and lithologic controls at Storm and is primarily located within breccias found along the upper stratigraphic contact of the Bootstrap Limestone and within or peripheral to highly

permeable fault zones that cut massive limestone. Geochemical analysis on drill holes shows a decrease in calcium with a significant addition of magnesium, manganese, and iron between the fresh sparry limestone and hydrothermal dolomite. The addition of iron during the dolomitization process was critical for later sulfidation of these carbonate units by gold-bearing ore fluids. Routine carbonate staining of core (e.g., Hitzman, 1999) suggests that the majority of dolomite at Storm is indeed ferroan, generally displaying a violet-blue color. Local rare zebra dolomite fragments have been identified within dolomitized limestone breccias in the 49'er Zone but are not nearly as volumetrically significant as those found at the Meikle mine (Evans, 2000).

In hand sample, hydrothermal ferroan-dolomite appears tan to buff in color due to bleaching effects associated with the removal of organics during the dolomitization process. The conversion of primary calcite to hydrothermal dolomite creates a volume reduction along fluid pathways and within breccia bodies that increases the permeability and porosity for later pulses of hydrothermal fluids. Overprinting of hydrothermal dolomite alteration by subsequent hydrothermal events is generally texturally destructive and may even result in the removal of dolomite from the rock. The best preserved ferroan dolomite-rich crackle breccias have had the matrix material replaced by silica.

The development of hydrothermal dolomite at Meikle has been linked to a base metal mineralizing event that presumably occurred sometime during the Paleozoic (Evans, 2000). Although Storm shows no sign of a base metal event or Mesozoic aged dikes that cut dolomitized limestone, it is possible that the dolomitizing fluids are of similar age and source. What is known is that brecciation and dolomitization are essential stages of rock preparation that control ore-fluid dynamics as well as the

geometry, size, and distribution of orebodies at Storm. Therefore, zones that contain thick intervals of dolomite-dominated breccia are the primary exploration targets at Storm and the surrounding areas.

Decarbonatization: Decarbonatization of both primary carbonate material as well as hydrothermal dolomite is restricted to areas within and proximal to fluid pathways (i.e. faults, stratigraphic contacts, igneous dikes, etc). Within brecciated zones the intensity of decarbonatization is generally zoned outward from mineralization, where there is generally a complete dissolution of carbonate material. Carbonate content increases with proximity to massive Bootstrap Limestone and the effects of decarbonatization rarely penetrate more than a few meters into the massive sparry unit unless focused along faults or intrusive igneous bodies. Lateral flow of hydrothermal fluids along stratigraphic boundaries, such as the Bootstrap-Popovich and the Bootstrap-Roberts Mountains formation contacts, can extend decarbonatization hundreds of meters from major fault zones. Thin, laterally extensive collapse breccias form along these boundaries and locally thicken at intersections with high angle structures. Mineralization at Storm has an inverse relationship to calcium content of the rock. The highest gold grades are almost exclusively found in decarbonatized rocks containing less than 2 wt. % calcium (Fig. 12).

Paragenetically, decarbonatization occurred concurrently with sulfidation (pyrite deposition) prior to the first silicification event at Storm. The aerial extent of decalcified rock is unknown, although decarbonatized fragments are locally observed within most breccia bodies. The effects of overprinting alteration such as silicification, sulfidation,

and argillization locally destroy and/or mask most decarbonatization features such as effervescence when contacted with hydrochloric acid.

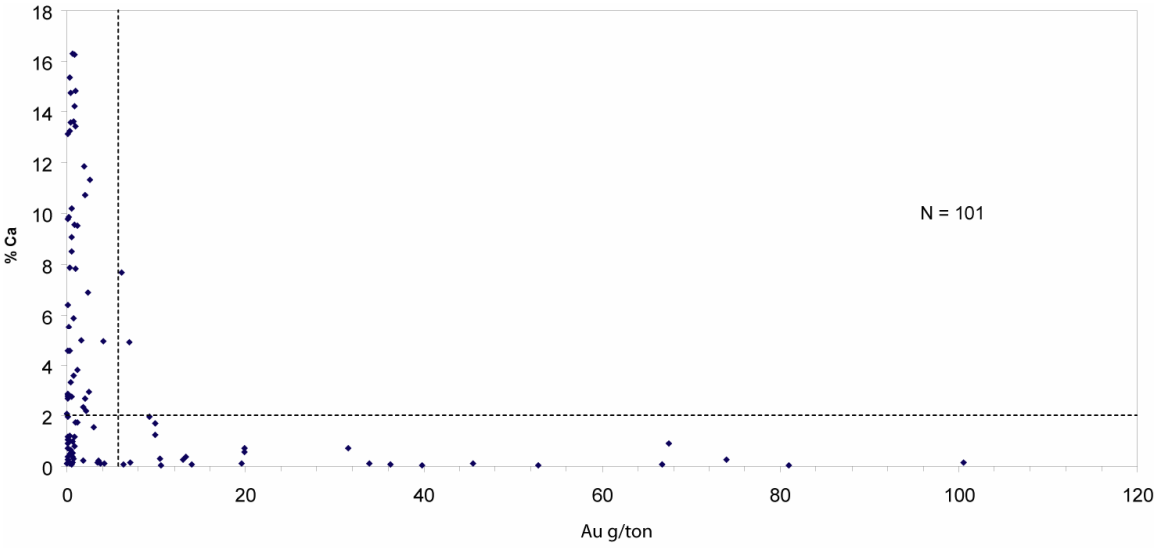

Figure 12. Plot showing calcium concentration (wt.%) versus gold grade (g/ton). Note that the majority of ore grade material (>6.25 g/ton) occurs in decarbonatized rock with calcium levels below 2 wt.%.

Silicification: Silicification is a primary type of hydrothermal alteration present in all Carlin-type deposits, although the intensity and temporal relationship to gold mineralization generally ranges within and between individual deposits (Arehart, 1996). At Storm, silicification is spatially and temporally associated with Carlin-type gold mineralization. Intense silicification and jasperoidization (near complete replacement by silica) is centered on the main orebodies and is zoned outward in all directions. Typical ore zones have a substantial silica component (>75%) and metallurgical studies have shown that silica encapsulation of gold ranges between 72 and 81% (Barrick internal report, 2001).

Jasperoid formation occurs in zones localized along high-angle structures and extends laterally along stratigraphically controlled breccia bodies. Highly permeable breccia bodies provided adequate fluid-rock interaction that allowed for near complete replacement of original carbonate material by quartz. Inclusions of relict carbonate grains, chemically resistant iron-hyroxide impurities, and abundant <5 micron-diameter fluid inclusions give the jasperoids a cloudy or dusty appearance when viewed microscopically (Fig. 13). Quartz grains are typically aggregates of microcrystalline and crystalline quartz crystals (0.05 – 0.20mm diameter) that have irregular and interpenetrating crystal boundaries. Differences in grain size could possibly reflect inherited morphology of the original replaced minerals (Lubben, 2004). Encapsulation of pre-ore and gold-rich pyrite by jasperoid suggests that silicification was main stage Carlin-type mineralization.

Sulfidation: Two stages of sulfidation have been recognized at Storm, although the timing and extent of each event are only loosely constrained. The flow of fluids, rich in reduced sulfur (or sulfide), within structures and breccia bodies allowed for sulfidation of hydrothermal ferroan-dolomite and resulted in the widespread creation of pyrite. Up to 5% pyrite is common within all the major ore zones, much of which is attributed to this stage of sulfidation. Sulfidation of iron-bearing silicates within Jurassic lamprophyre dikes and dike fragments is common and can locally result in up to 10% pyrite. The possibility exists that the hydrothermal fluids responsible for this stage of alteration are related to late Jurassic polymetallic mineralization found at the Betze deposit (Emsbo et al., 2000).

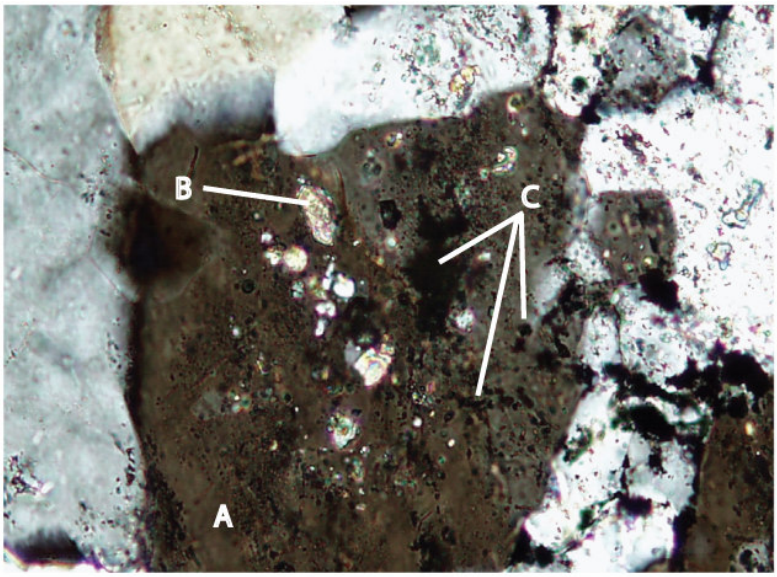

Figure 13. Inclusions of carbonate and iron-hydroxides within Carlin stage jasperoids. A=Quartz; B=Calcite; C=Fe-hydroxides. Plain light photmicrograph (XP) with a 0.85 mm field of view.

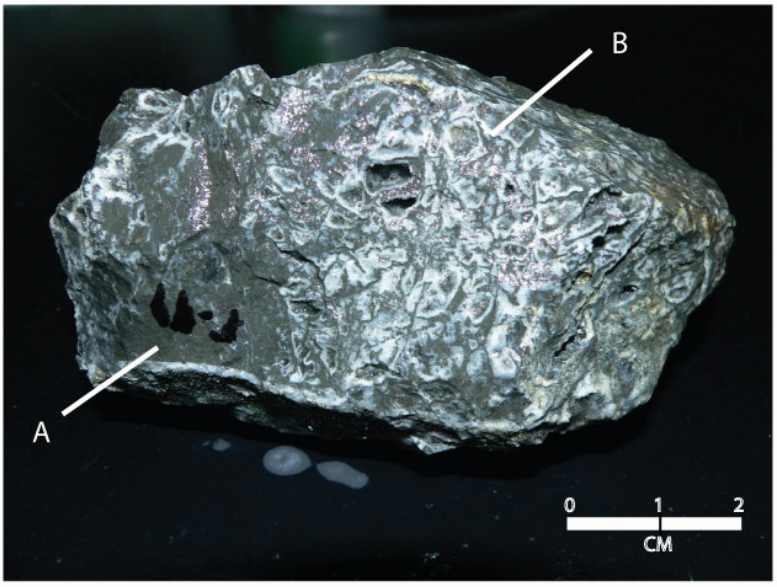

Figure 14. Grab sample from the 49'er cross-cut. Sample contains 15.86 g/ton gold. Rock is comprised of fine grained silica and sulfide material (A) cut by post-Carlin white quartz (B).

The second stage of sulfidation occurred during the main formation of the Carlin-type gold and resulted in the precipitation of arsenic and gold-rich rims on pre-existing pyrite grains. Replacement of entire grains of pyrite by gold-rich pyrite occurred, including within both the lamprophyre dikes and main orebodies.

Argillization: Documented argillization at Storm is limited to igneous dikes as the carbonate host rocks for most of the deposits lack any primary silicate material. Kaolinite and dickite replace primary igneous phenocrysts and groundmass within the lamprophyre dikes. In hand-sample, strongly argillized lamprophyre is light colored and the hornblende phenocrysts, which are altered to clay, are tan to white.

Mineralization Characteristics and Distribution

The mineralized zones at Storm are the unoxidized down dip extensions of the Dee and Dee-Deep North orebodies and occur at depths of 220 to 480 meters below the present surface. The three economic orebodies include, in order of decreasing depth, the 49'er, End, and Discovery zones. Orebody geometries and the intensity of gold-silver mineralization are linked to controlling faults. The Dee, Hinge, and End Zone faults all contain mineralized zones that commonly parallel the fault strike. Low levels of precious metals and trace elements, such as As, Sb, Hg, and Tl, are present within most minor faults at Storm, but structures with thick (>5m) zones of breccia tend to be preferentially mineralized.

Storm ore is characterized by dense silica-sulfide replacement bodies that consist almost entirely of fine-grained quartz and up to 5% disseminated sulfides (Fig. 14). Ore-grade material has an economic cut-off grade of 6.2 g/t gold but the average grade of the orebodies exceeds 12.4 g/t. The difference between economic grade mineralization and sub-economic rock is clearly visible and can locally be knife-edged. High-grade samples commonly contain dense patches or clots of sulfide that exhibit a green tint when viewed with a hand lens; Barrick geologists have coined this "bronzy" pyrite. Unlike many other Carlin-type deposits Storm lacks both orpiment and realgar.

Figure 15a is a cross-section through the 49'er Zone deposit and shows the distribution of gold within the breccias associated with the Dee fault, the controlling structure for mineralization. Even low levels of gold are entirely bound by zones of

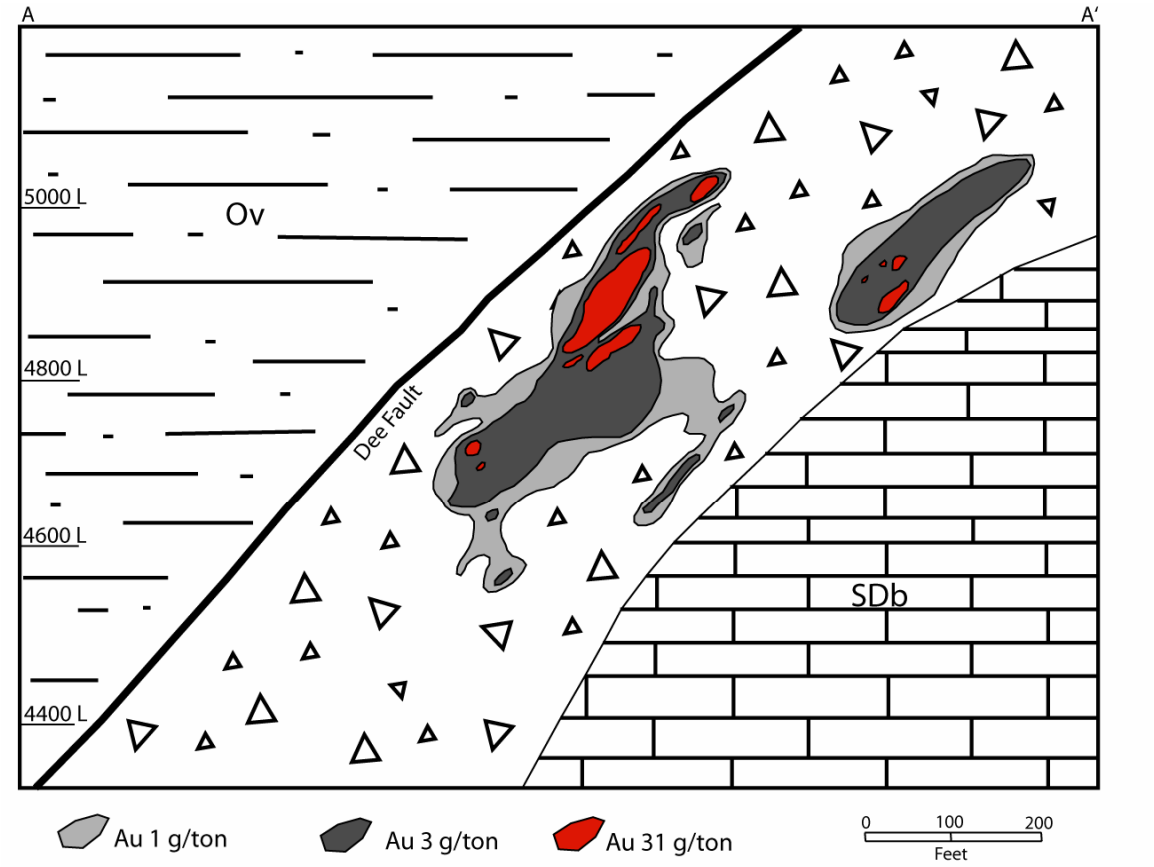

Figure 15a. Schematic cross-section through the 49'er deposit illustrating gold grade distributions. Gold values are found exclusively within breccias (tectonic and collapse) in the footwall of the Dee Fault. Section is looking N10W and the surface trace of this section can be seen on Figure 3. Note that cross-section does not extend to surface.

tectonic and collapse breccia. The level at which the dominant lithology changes from dolomite to mudstone is the focus of the highest grade mineralization. Ore fluids moving upwards along these faults pond beneath the mudstone-rich breccias near the top of the

breccia piles and these mudstone breccias act either as a barrier to fluid flow or are less reactive than the iron-rich dolomite rocks beneath.

Figure 15b shows the distribution of silver through the 49'er Zone deposit and shows a strong spatial association between gold and silver mineralization. Unlike gold, silver mineralization is found throughout the entire breccia pile. Low-grade silver mineralization locally bleeds upwards into the mudstone-dominated portion of the tectonic breccia, although this distance is no more than gold travels. Silver is also found penetrating altered and jointed limestone near the upper limits of the Bootstrap Formation.

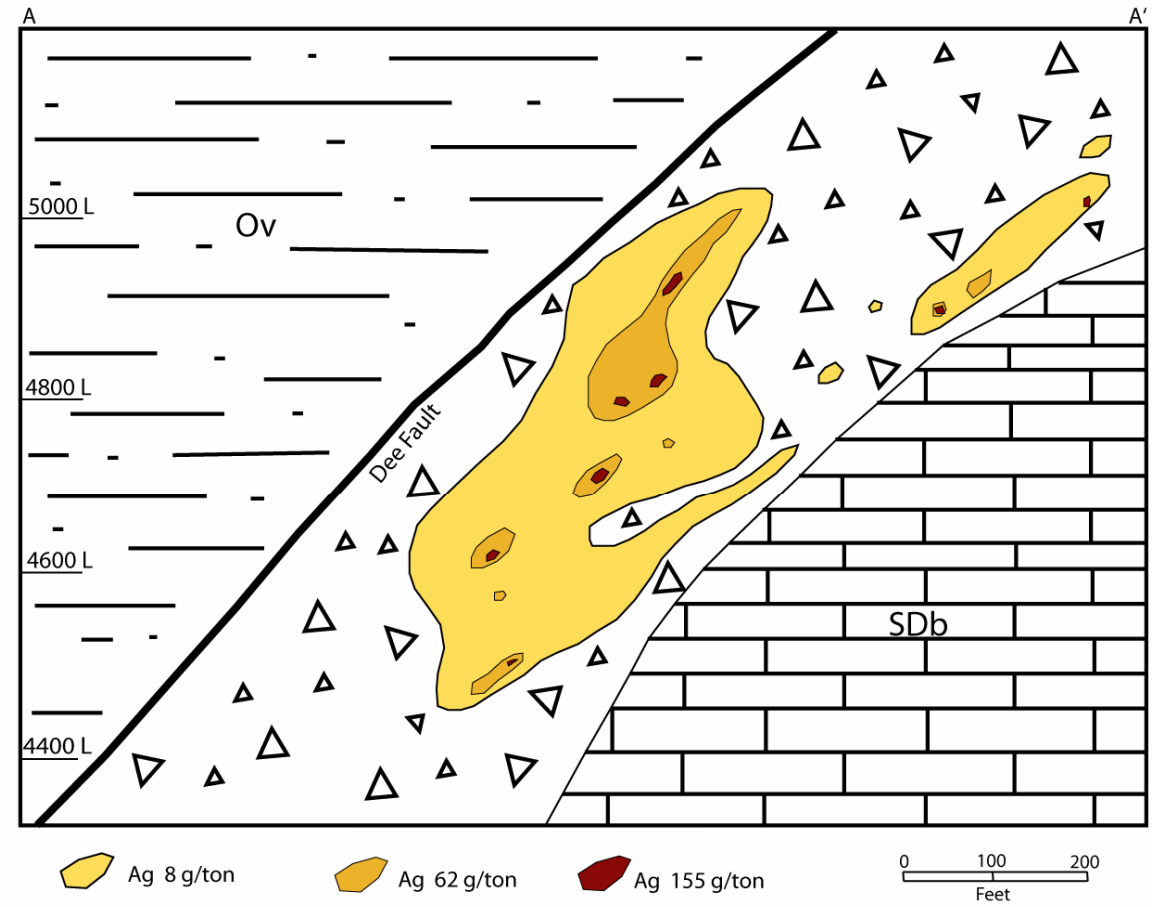

Figure 15b. Schematic cross-section through the 49'er deposit illustrating silver distribution. Section is looking N10W. Note that cross-section does not extend to surface.

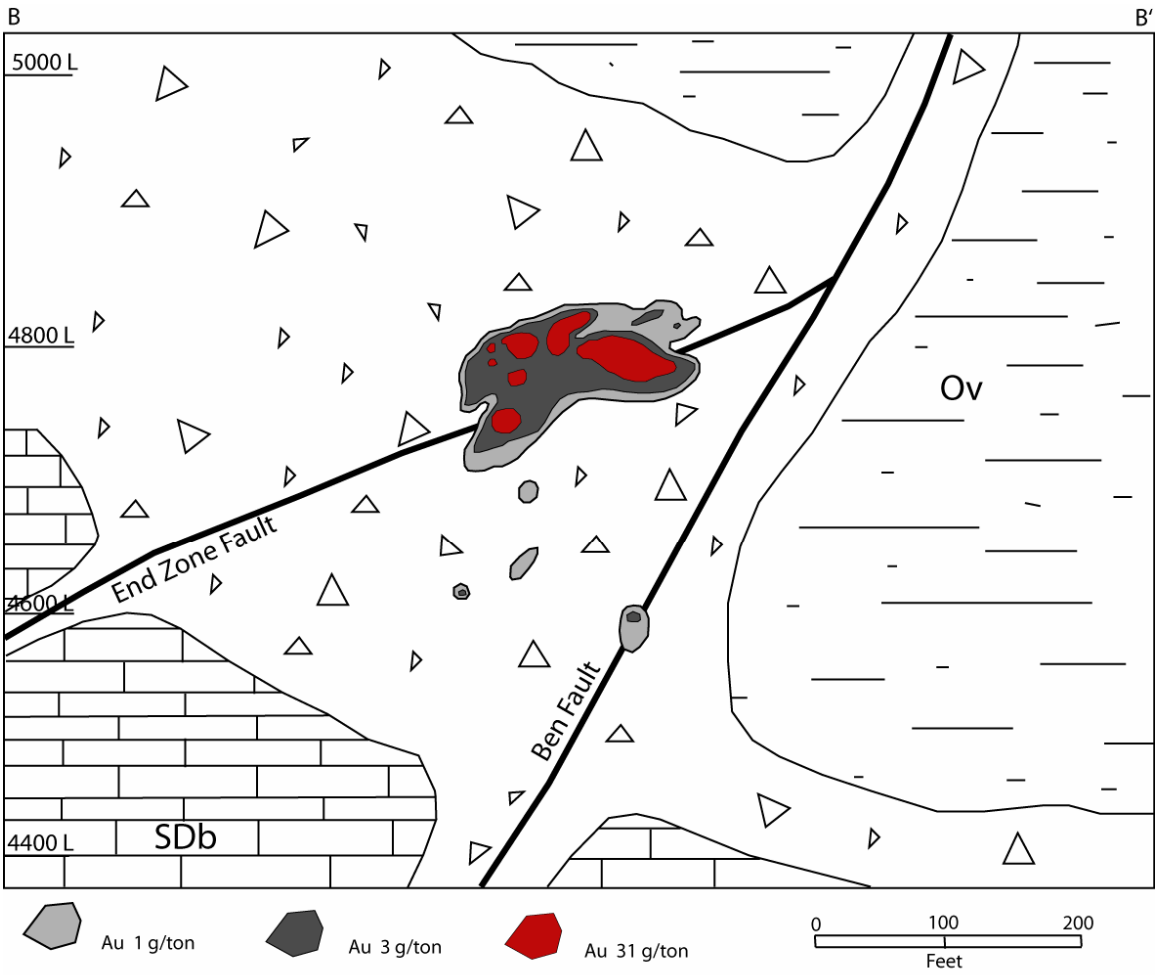

FIgure 16a. Schematic cross-section through the End Zone deposit looking N50E. This deposit is entirely breccia hosted (tectonic and collapse) and the primary control on gold mineralization is the End Zone Fault, which dips into the page at approximately 55-60 degrees. Note that cross-section does not extend to surface.

Unlike the 49'er Zone, the breccias found within the End Zone (Fig. 16a) have a far more complex nature and are comprised of a mixture of large-scale collapse breccias and tectonic breccias. Both gold and silver grades (Fig. 16a, b) are highest where faults intersect collapse breccias.

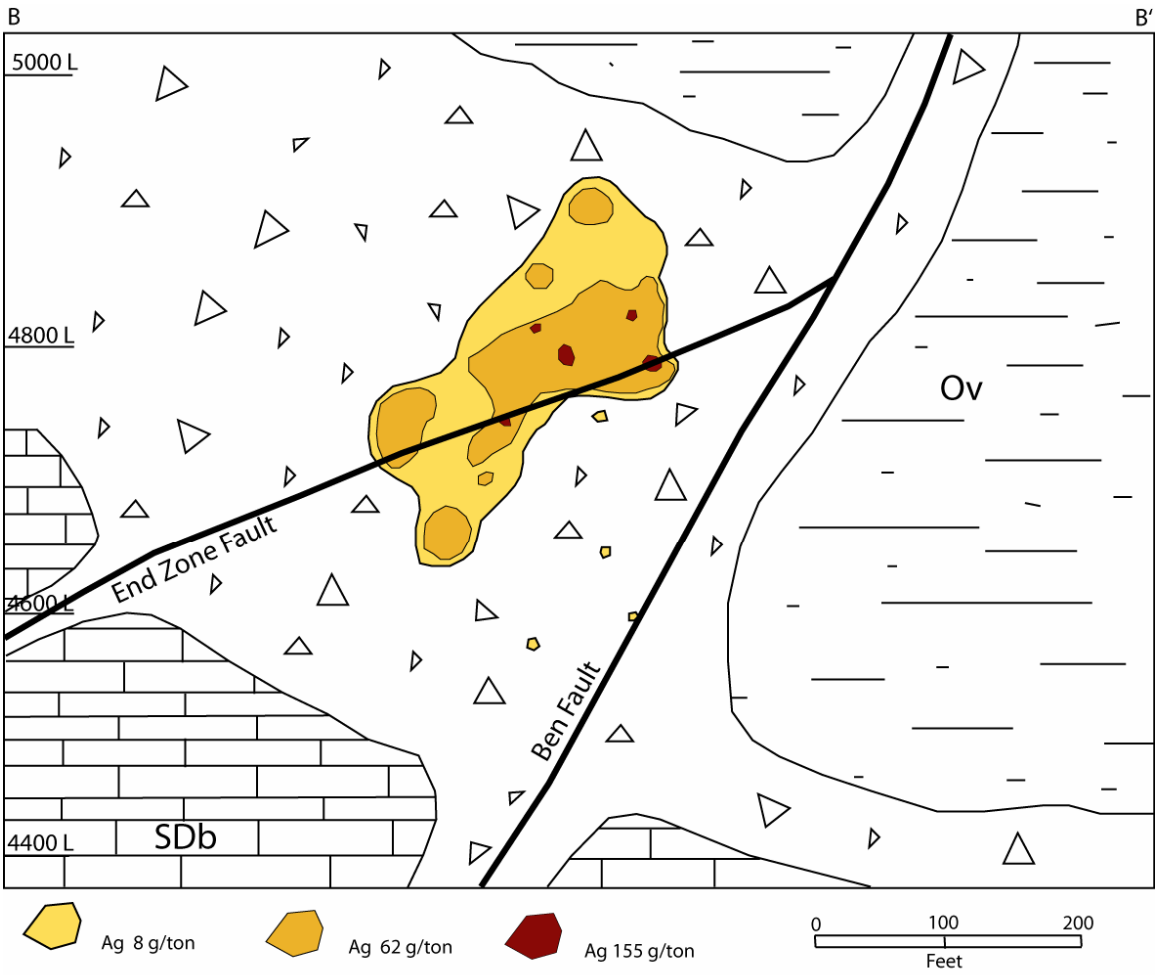

FIgure 16b. Schematic cross-section through the End Zone deposit looking N50E. This deposit is entirely breccia hosted (tectonic and collapse) and the primary control on silver mineralization is the End Zone Fault, which dips into the page at approximately 55-60 degrees. Note that cross-section does not extend to surface.

Mineralogy and Mineral Paragenesis

A wide variety of mineral assemblages are present at Storm, including electrum, sulfides, sulfosalts, selenides, and gangue phases. Six stages of mineral deposition have been identified at Storm. They are: (1) pre-Carlin-type mineralization, (2) gold-dominant Carlin-type ore formation(3) post-ore Carlin-type quartz-stibnite veining, (4) post-ore silver-dominant low-sulfidation epithermal vein style mineralization, (5) post-ore collapse brecciation and veining, and (6) supergene oxidation. A comprehensive paragenetic sequence for ore and gangue minerals found within the Storm hydrothermal system is shown in Figure 17.

Pre-Carlin: The pre-Carlin mineralization includes diagenetic pyrite, hydrothermal ferroan-dolomite, and pyrite associated with the first stage of sulfidation. Pre-Carlin mineralization is interpreted to have formed significantly before Carlin-type mineralization, prior to the Tertiary. Mudstone units of the Rodeo Creek and Vinini formations both contain ranging quantities of diagenetic framboidal and cubic pyrite. Both pyrite morphologies form in linear bands/pods that are locally parallel to bedding planes. Framboidal pyrite (Fig. 18a) consist of aggregates of numerous small 1-3 μm euhedral crystals with good polish and relief that accumulate in small circular shaped clusters averaging 10-20 μm in diameter. The second variety of diagenetic pyrite forms mostly cubic to locally anhedral crystals 20-120 in diameter (Fig. 18a). They hold a good polish, have high relief, and contain local pore spaces. None of the framboidal or cubic

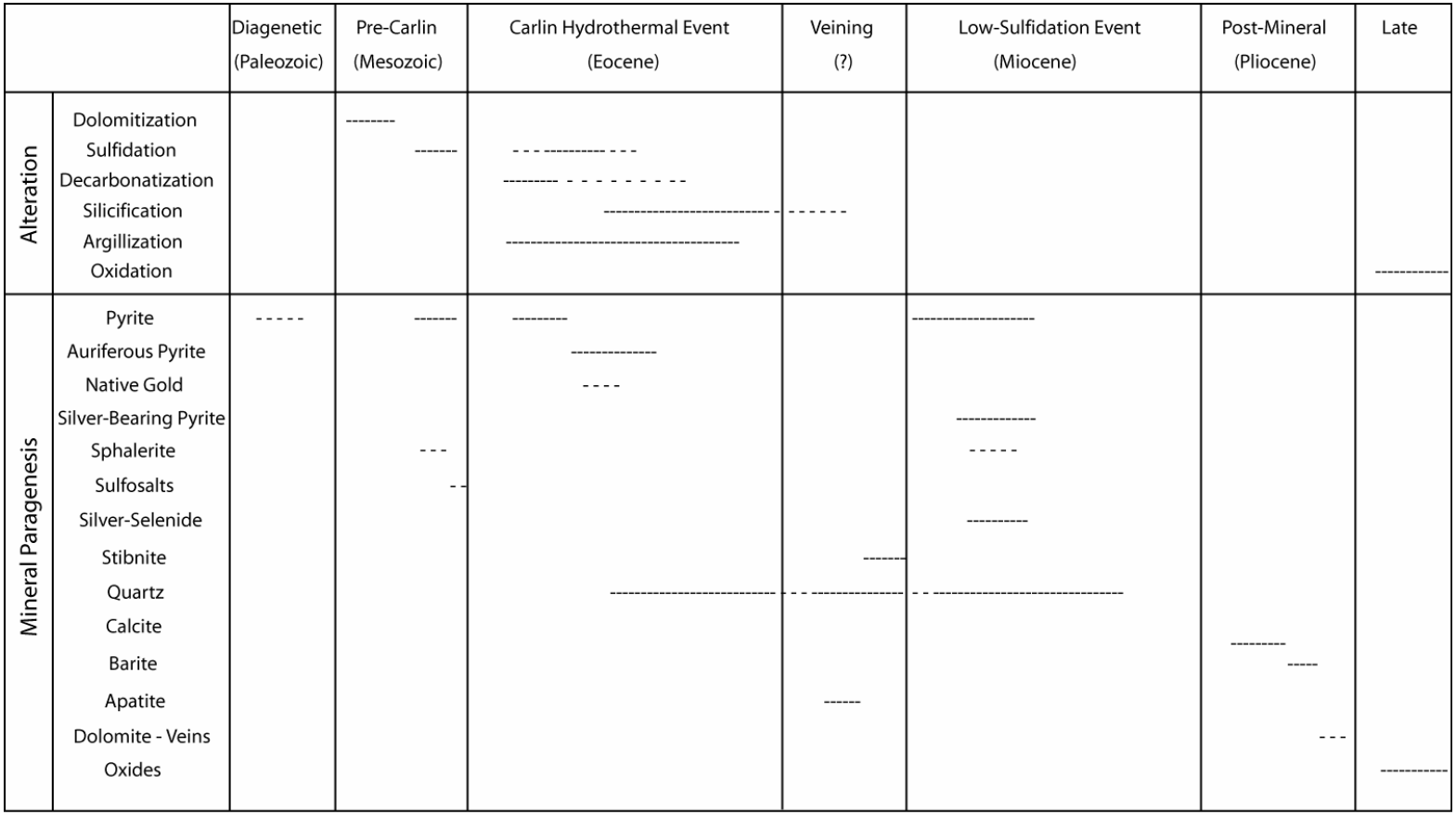

Figure 17. Paragenetic diagram characterizing both alteration events as well as individual mineral paragenesis at Storm.

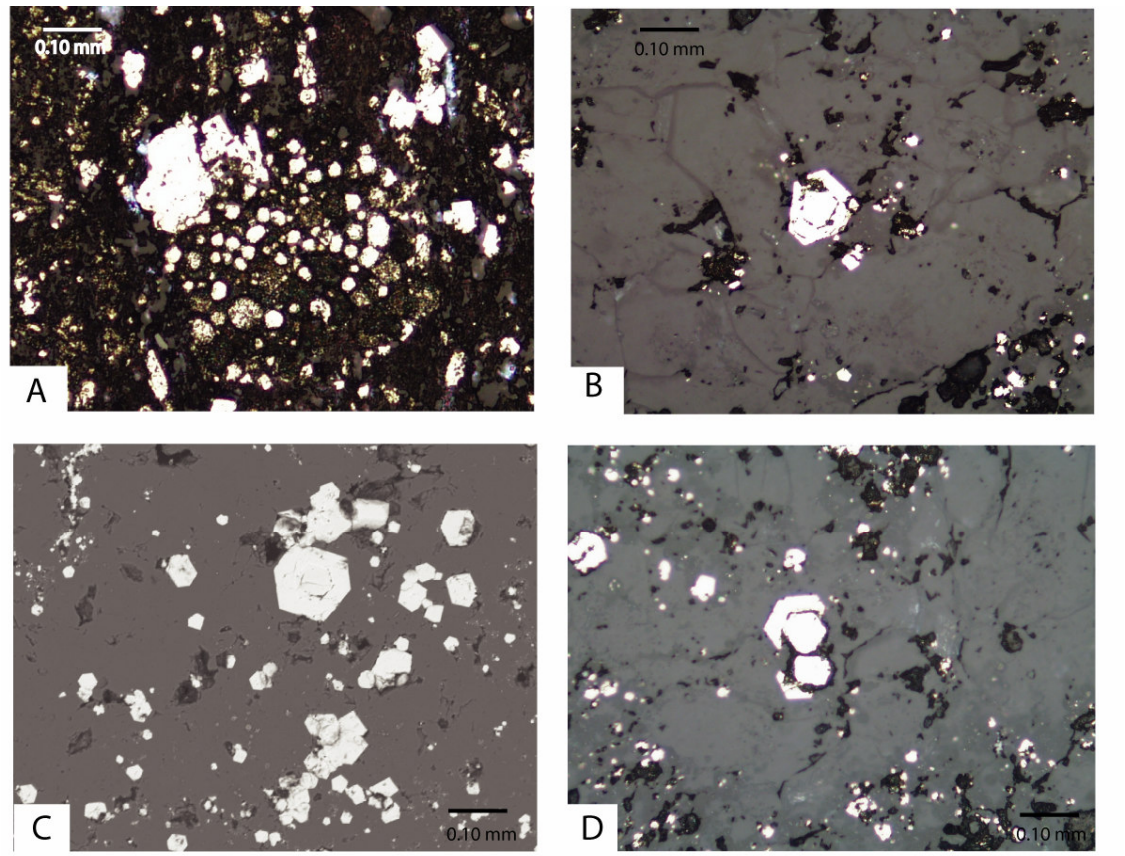

Figure 18. Photomicrographs of various diagenetic and hydrothermal pyrites of a pre-Carlin nature. A. Diagenetic pyrite in mudstone of the Rodeo Creek Formation. B. Euhedral pre-Carlin pyrites in jasperoid. Two growth zones are clearly visible. C. Back-scatter image of pre-Carlin pyrite. D. Common feature in pre-Carlin pyrite is the dissolution of the outer, inner, or both growth rims. All photomicrographs have are viewed in reflected light and have a field of view of 0.85mm.

pyrite observed in this study had any stages of overprinting pyrite rims, nor was there any evidence of diagenetic pyrite within the Bootstrap Formation.

Primary carbonates of the Bootstrap Formation are consistently altered to hydrothermal ferroan-dolomite where structures intersected areas of high permeability and porosity, namely breccia bodies and stratigraphic contacts. Ferroan-dolomite, where preserved, forms 0.05 to 0.1 mm anhedral to euhedral rhomb-shaped crystals. The vast

majority of dolomite has been completely replaced by a combination of silica and sulfides.

Euhedral pre-ore pyrite deposition is associated with hydrothermal alteration (sulfidation) of pre-existing Fe-rich minerals and occurs in both igneous and sedimentary rocks throughout the deposit. Pre-ore pyrite is the most abundant variety of pyrite at Storm and is locally associated with dark brown to black iron-rich sphalerite. Common psuedomorphic replacements in the Jurassic lamprophyre dikes include Fe-rich minerals such as hornblende, pyroxene, and biotite.

Pre-ore pyrites are generally euhedral to subhedral crystals or aggregate masses 20-100 μm in diameter, have relatively high polished relief, and hold a clean polish. Morphologies include both cubic and pyritohedral-shaped crystals (Fig. 18b). Pyrites can have both massive and porous textures. Single growth zones are locally present and generally equally proportioned between the inner and outer zones (Fig. 18b, c). Later alteration has locally resulted in partial dissolution of the outer, inner, or a combination of both growth zones (Fig 18d). Quantitative microprobe analysis of pre-ore pyrites shows they are barren of precious metals but have anomalous concentrations of As in the outer growth zones. Inner zones consistently display As levels well below detection limits of the analyzing equipment compared to 0.4 – 1.3 wt. % As in outer zones. Both zones contain variable concentrations of Zn and Cu ranging from 200 - 500 gram/ton and Hg ranging from 400 – 2000 gram/ton. Other trace elements such as Sb, Tl, Te, and Se were all below detection limits.

Sulfosalts of various compositions are commonly found replacing dark colored sphalerite (iron-poor) throughout the Storm deposit. Both the sphalerite and various

sulfosalts are presumed to be part of a late Jurassic hydrothermal event and are overprinted by Carlin silicification. Sulfosalts found in Storm have variable compositions, although most are precious metal bearing. To date, three distinct phases have been identified based on compositional differences and include:

(1) Sb (25.5%) - S (21.5%) - Cu (23.1%) - Ag (17.0 %) - Hg (9.8%) - Zn (2.4%)
(2) S (24.2%) – Cu (28.8%) – Sb (19.2%) – Ag (9.2%) – As (6.1%) – Zn (5.5%)
(3) Hg (37.4%) – S (12.0%) – Te (10.2%) – Zn (10.0%) – Sb (6.8%) – Au (0.65%)

The first two varieties have been documented with reflected light microscopy as partial replacements of sphalerite and as individual grains, while the tellurium bearing sulfosalt has only been identified using a microprobe and occurs only as a replacement mineral after sphalerite.

Carlin Event: The primary stage of mineralization at Storm consists entirely of trace element-rich pyrite. Sub-millimeter rims of gold- and silver-rich arsenian pyrite, fine-grained aggregate masses, as well as entire subhedral to euhedral grains have been documented replacing pre-ore stage pyrite. The caustic nature of the ore fluids has caused partial to complete dissolution of the pre-ore stage pyrite crystal boundaries prior to or coeval with the deposition of the mineralized rims (Fig. 19). This reaction creates a porous zone between the main-stage pyrite rim and the pre-ore pyrite that appears mottled when using reflected light microscopy. The fine-grained masses are associated with the main-stage pyrite rims and may represent the complete replacement of fine-grained pre-ore pyrites. Under reflected light both the main-stage pyrite rims and fine-

grained masses locally have a distinct steel-blue tint that makes them easily distinguishable from the pre-ore pyrite (Fig. 19).

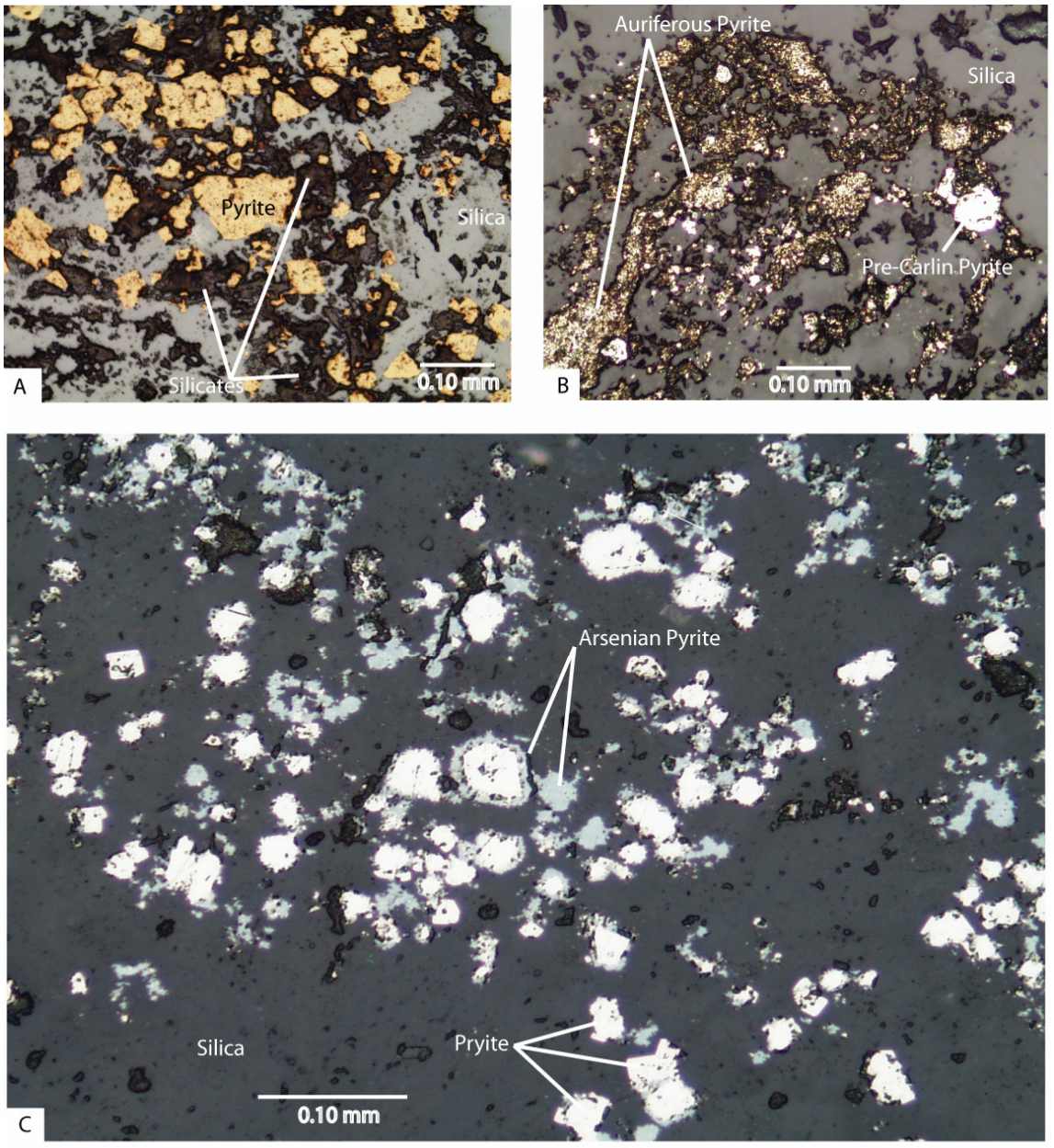

Figure 19. Photomicrographs of various gold bearing Carlin stage pyrite morphologies. A. Sulfidized lamprophyre dike containing subhedral gold-bearing pyrite psuedomorphs of primary iron-bearing minerals. B. Clusters of anhedral ore-stage pyrite replacing pre-Carlin barren pyrite grains in a jasperoid. C. Gold-rich arsenian rims (steel blue) on pre-Carlin pyrite (white). All pictures have a 0.85 mm field of view and were taken in reflected light.

The main stage pyrite generations have a distinct geochemical signature when compared to other Fe-sulfides at Storm. Microprobe analyses show a large assemblage of trace elements and precious metals including (in decreasing abundance) As, Sb, Cu, Au, Ag, Hg, Zn, and Te. Overall, there is a pronounced increase in trace elements from the pre-ore pyrite to the main-stage replacement pyrite. Two analyses were successful in quantifying the chemistry of main-stage pyrites and the results are presented in Table 1. Other analyses returned low total mass (<80%), possibly due to silica encapsulation, and were not reported. Although the sample suite is not sufficiently large to accurately gauge the gold to silver ratio of the main-stage Carlin hydrothermal event, it does suggest a slightly lower ratio (~2 to 1) than is commonly seen in other deposits, which is generally greater than 4 to 1.

Sample#	Location	Fe	S	As	Sb	Cu	Au	Zn	Te	Ag	Tl	Hg	Total
ES53-1	Rim A	47.46	34.38	2.12	1.12	2630	1380	570	230	1310	bdl	1930	86.453
ES53-1	Core A	44.97	52.49	0.52	0.01	bdl	bdl	bdl	bdl	bdl	bdl	148	98.221
ES53-1	Rim B	42.59	47.33	4.16	0.46	3170	3120	370	160	1050	bdl	1350	96.018
ES53-1	Core B	44.69	52.56	0.46	bdl	300	bdl	200	bdl	bdl	bdl	240	97.918

Table 1. Results from quantitative micorprobe analyses of main-stage pyrite rims and pre-ore cores. Fe, S, As, and Sb are all reported in wt.% and Cu, Au, Zn, Te, Ag, Tl, and Hg are all in ppm.

Native gold is a common constituent of ore-grade material and is used by Barrick geologists as an indicator of the overall grade of the rock, as it is generally seen in mineralized intervals grading at least 0.3 oz/ton gold or higher. Native gold only

accounts for a small fraction of the recoverable gold at Storm. The grains typically range from 0.1 to 0.3 mm in diameter in hand sample but have been documented up to 2 mm

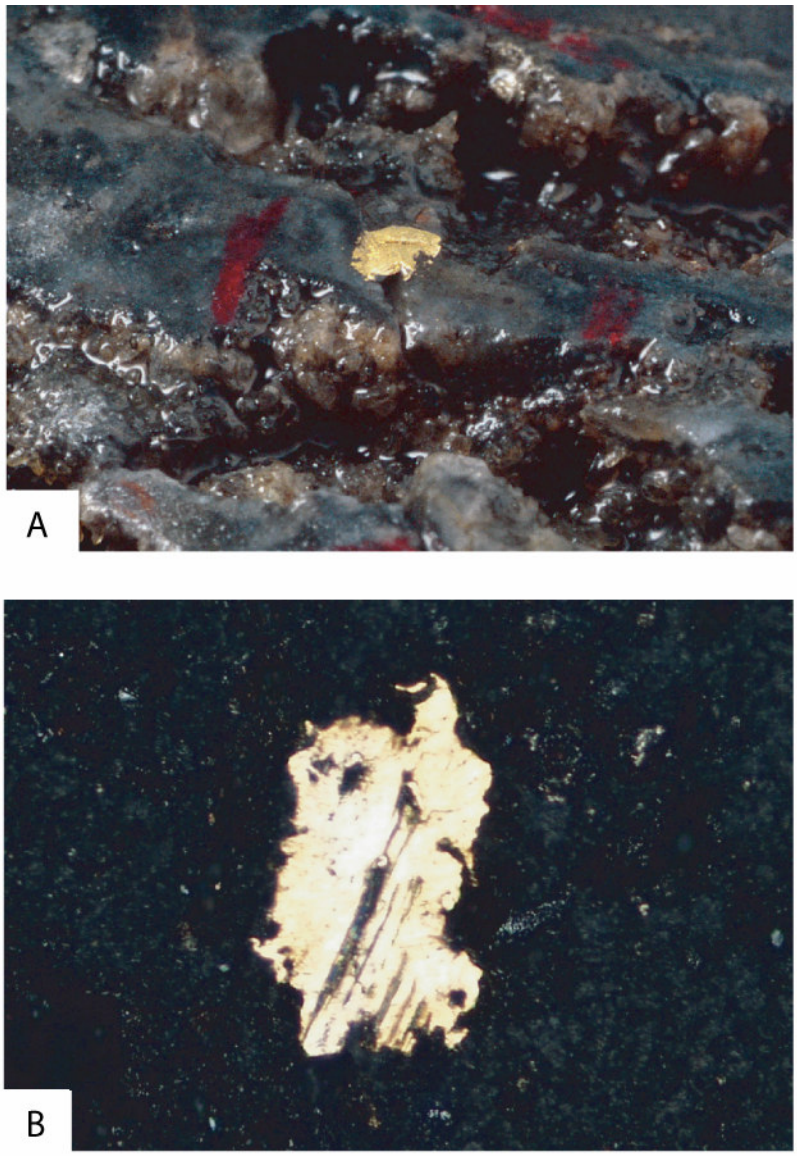

Figure 20. Visible gold present at Storm. A. 2mm gold grain located in a fracture in a silicified and sulfide-rich breccia. Red streaks are marker outlining the gold grain. Gold grain has been partially smeared by drilling. B. Photomicrograph of a gold grain in a densely silicified and sulfide-rich breccia. Reflected light with a field of fiew of 2mm.

(Fig. 20). Gold grains are generally found disseminated throughout the sulfide-rich ore zones. The best microprobe analysis of a single gold grain showed it contains approximately 84.9% gold and 9.7% silver. The total recovery on this run was 96.2%. These grains are only observed in areas that contain high gold grades as well as strong silicification (jasperoidization). In fact, the reason only one microprobe analysis has been reported is due to the fact that native gold is generally encapsulated by silica and/or the grain is thin enough that the microprobe beam penetrates it and analyzes the underlying quartz. Microprobe analyses of native gold grains from oxidized zones were unsuccessful due to the high degree of silica interference with the analyzing beam. While the exact chemical makeup of the gold grains in oxidized zones is unknown, microscopic analysis has indicated that the grains occur within small patches of sulfide material. This suggests that the majority, if not all, of the Au^{o} at Storm is hypogene in origin and that the encapsulating silica is related to post Carlin jasperoid.

Post-Carlin: Post-ore jasperoid is the last stage of Carlin hydrothermal activity at Storm. It is largely associated with intense silicification and jasperoidization of the sulfide-rich portions of the breccia bodies. Nearly complete silica encapsulation of main stage and pre-ore pyrites suggests the silicification occurred after the deposition of Carlin-type gold ores. Jasperoidization was widespread throughout the deposit and decreases intensity laterally away from the tectonic breccia zones into the collapse breccias found along stratigraphic contacts.

Following the late-stage Carlin silicification Storm underwent a stage of intense quartz veining and associated stibnite mineralization. Discreet 5 mm to 5 cm wide quartz ± stibnite veins cut Carlin mineralization, including jasperoids, and occur in close

proximity to ore zones. These veins are typically crustiform with comb-textured euhedral crystals up to 2 cm in length. The medial portions of these veins are locally filled by massive stibnite, although euhedral crystals up to 5 mm in length have been noted in small vugs within the veins (Fig. 21). Where these veins cut silicified rock, including mudstones, they tend to have sharp, matching vein walls with no apparent alteration selvage. Quartz-stibnite veins that cut non-silicified breccias tend to flood the pore space between clasts instead of forming discreet veins. Veins occurring in oxidized zones of the deposit are typically void of stibnite yet are locally observed to have prismatic shaped pits with trace stibiconite present. Light yellowish-green to clear euhedral apatite crystals are also associated with this silicification event and are locally seen as 80-250 micron grains within quartz.

Although the timing of this stage of silicification at Storm has been loosely constrained between the Carlin mineralization and subsequent silver-bearing vein mineralization, it is unclear whether this is a distinct hydrothermal event. Silicification with associated stibnite has been documented on the Goldstrike property (Lubben, 2004) and is related to the waning stages of Carlin mineralization, although not at quite the scale seen at Storm. Conversely, stibnite horizons at the contact between the Carlin gravels and lower plate rocks at Gold Quarry have been dated at 15-16 Ma and could possibly represent a similar aged event as the quartz-stibnite veining event at Storm.

Silver-Bearing Veins: Low sulfidation silver veins represent the main stage of silver dominated mineralization at Storm. These veins are less than 2 mm wide and contain silver-bearing sulfides and selenides (Fig. 22). Vein walls are matching, contain

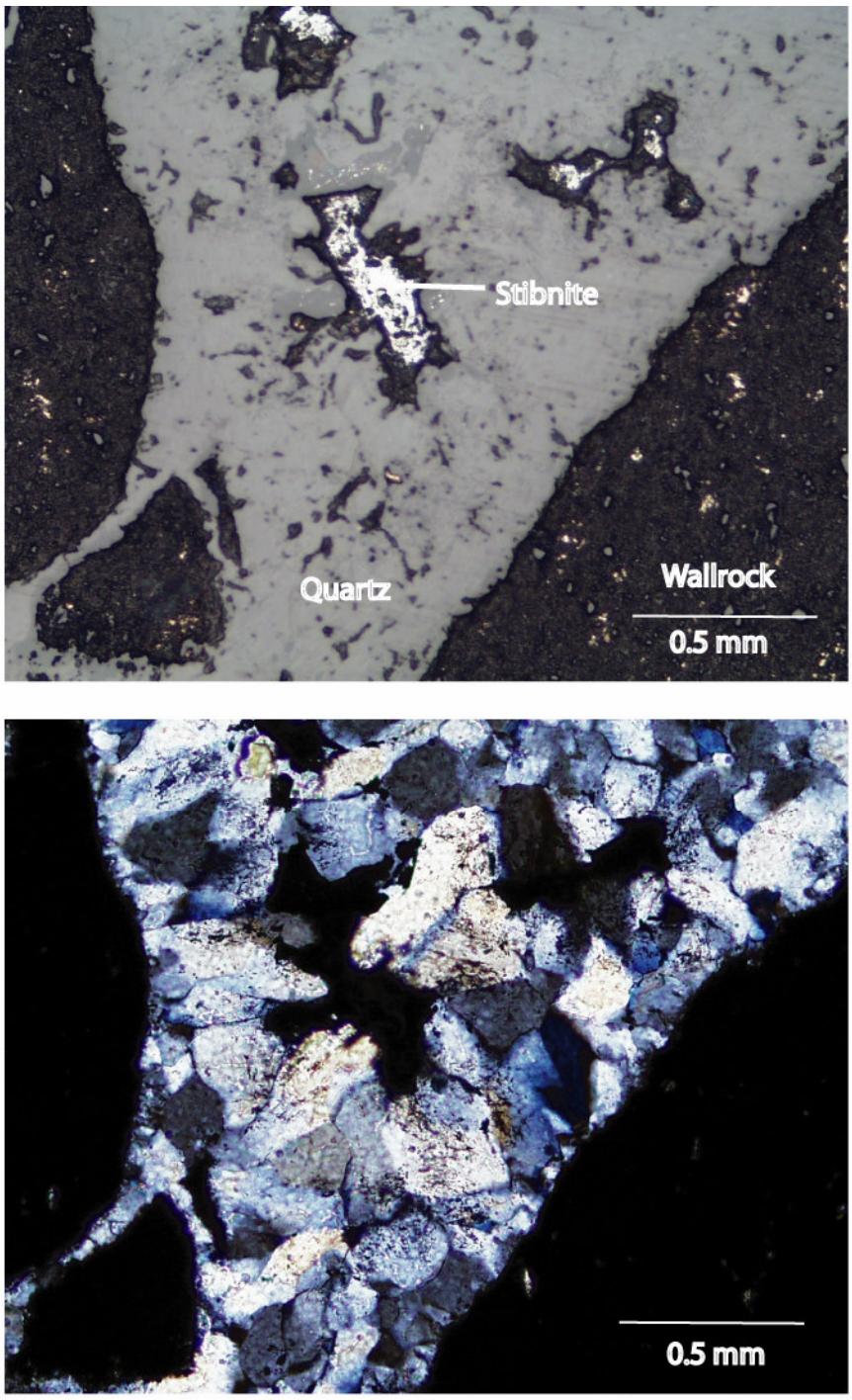

Figure 21. Quartz-stibnite veins cutting mudstone of the Rodeo Creek Formation. Stibnite occurs as infill within the medial portions of the quartz veins. Upper photomicrograph is in reflected light, the lower is plane light with XP. Field of view for both photos is approximately 2.2mm across.

no visible alteration selvage, and have at least two generations of quartz which are present within distinct vein bands. The first generation forms a thin (~25% of vein thickness) band of clear subhedral to euhedral crystals. The medial portion of the vein consists of euhedral sulfides crystals and anhedral quartz (Fig. 22b,c).

Silver- and antimony-rich pyrite locally form colloform crystals that radiate concentrically from vein walls and contain at least two growth zones. Antimony concentrations within (Fig. 22c) these pyrites are 1.8 to 5.0% and silver ranges from 1120 to 9300 gram/ton. The grains are typically yellow under reflected light and contain alternating porous and homogenous growth zones. In cross-section they appear semi-circular and have concentric bands showing the same relationship between porous and homogenous growth zones. In addition to rounded crystals, this same Sb-rich pyrite locally forms prismatic euhedra whose morphology suggests replacement of marcasite (Fig 22c).

Another common constituent of these silver-rich veins is an unidentified mineral that has a pseudo-cubic crystal habit (similar to argentite) and the following chemical components: 39% Ag, 38% Sb, 18% S, 5% Se, and minor amounts in both Hg and As. The deposition of this mineral is contemporaneous with the Sb-rich pyrite, as they typically occupy the same band within the quartz veins (Fig. 22c). Crystals range between 5 and 75 μm. Under reflected light, these crystals are typically seen as small tarnished grains with a light blue tint and look similar to argentite/acanthite.

A widespread episode of quartz-pyrite veining has been identified that cuts all mineralizing events (Fig. 23). These veins are 0.5 mm to 4 mm wide and are comprised

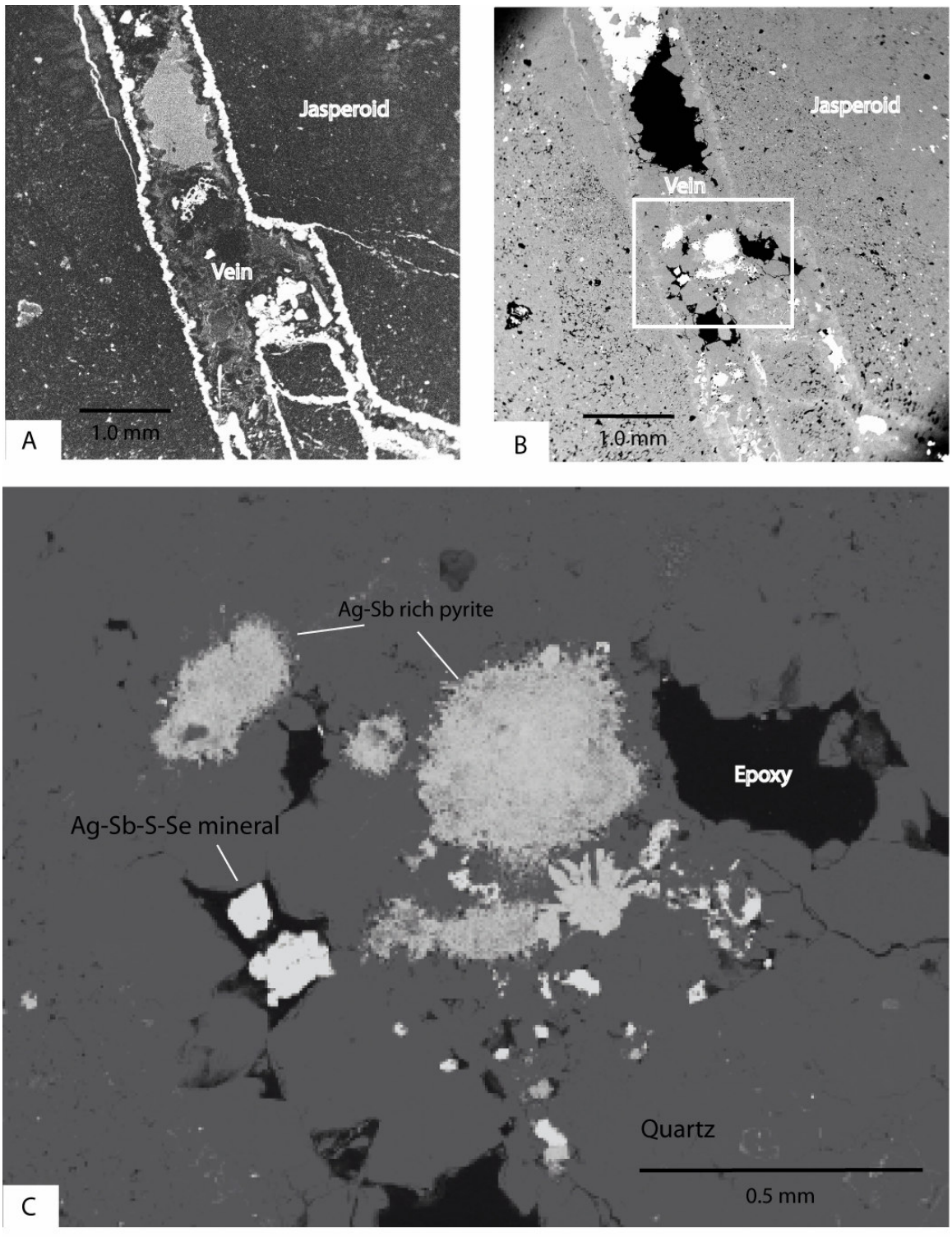

Figure 22. A. Cathodolumensence photomicrograph of Ag-Sb-Se vein cutting jasperoid. B. Half BSI - Half Cathodoluminescence photomicrograph (same field of view as A) illustrating sulfide material within the medial portions of the Ag-Sb-Se vein. C. Close-up from B (white box) of Ag-bearing ore minerals including: Ag and Sb-rich pyrite (light grey) and Ag-Sb-S-Se mineral with psuedo-cubic morphology (white). Field of view for photomicrographs A and B is 4.5 mm; C is 1.5 mm.

almost entirely of brassy colored anhedral pyrite. Where veins cut silicified breccias, widths are generally 0.5 mm to 1 mm compared to those found in unbrecciated mudstone units of the Rodeo Creek Formation, which are generally 1 to 4mm wide. Clear anhedral quartz is locally seen within these veins, although abundances never exceed 30 volume percent of vein material. Microprobe analyses have shown the pyrite to be particularly enriched in antimony, up to 3500 gram/ton, and contain silver concentrations only slightly above the analyzing machines' detection limits. The concentration of Hg, As, and Zn are all slightly elevated but never exceed that of antimony.

Post-Ore Collapse Brecciation and Veining: Massive calcite flooding and stockwork veining is common outboard the main mineralized zones and in post-mineral collapse breccias that may or may not contain displaced mineralized fragments. Calcite veins, typically less than 1 cm wide, locally blow out when they encounter zones of high pore-space, typically collapse breccia piles and vugs. Veins up to 1 meter thick have been locally observed. The veins are comprised of pure calcite and/or ankerite with rhombohedral crystals up to 2 cm in diameter. Local euhedral calcite forms as linings on open vugs. Cross-cutting relationships have shown the two carbonate veining types to be contemporaneous as both vein types are locally observed cutting each other. These veins cut all other silicified rocks.

Barite is commonly found with massive calcite as well as within voids in breccia bodies. Fault zones and vuggy silica zones are typically coated with massive white barite ± Fe-oxides, although collector quality crystal specimens have been historically

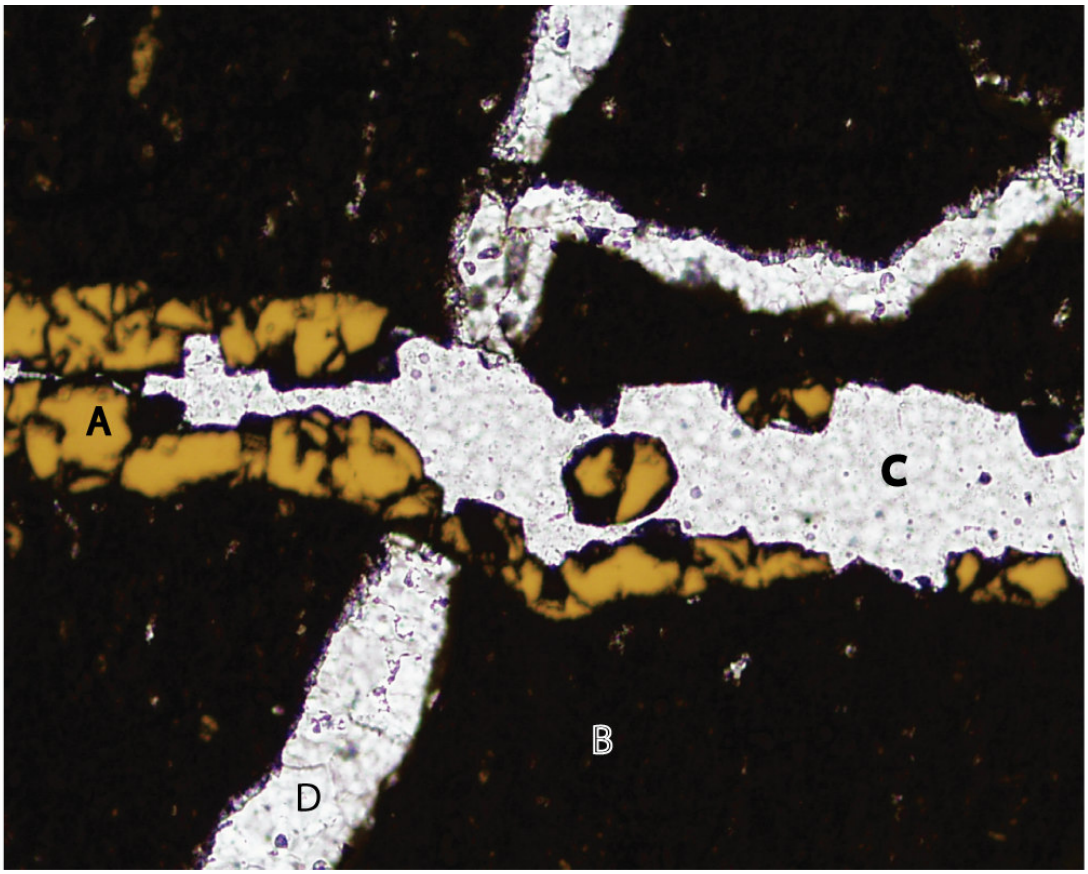

Figure 23. Late quartz pyrite vein cutting mudstone hostrock and an older generation of quartz veining. A=Pyrite; B=Mudstone; C=epoxy.; D=Quartz vein. Photomicrograph was taken in transmitted light with a field of view of 0.85mm.

produced from the Dee-Deep North workings. Similar high-quality barites have been encountered by current diamond drill campaigns. Large >2 cm honey-yellow barites have been observed as overgrowths on calcite in large vugs.

Late dolomite veining cross-cuts all other vein types and are generally seen as thin (1mm) stockworks, although local small scale vug-fillings have been observed. White rhomb shaped crystals up to 1 mm across are locally present within vugs and on fracture surfaces. These veins are commonly altered by later stage oxidation and acid leaching.

Supergene Oxidation: The final stage of alteration at Storm is related to the supergene oxidation of sulfides along permeable fault and fracture networks (Fig. 24).

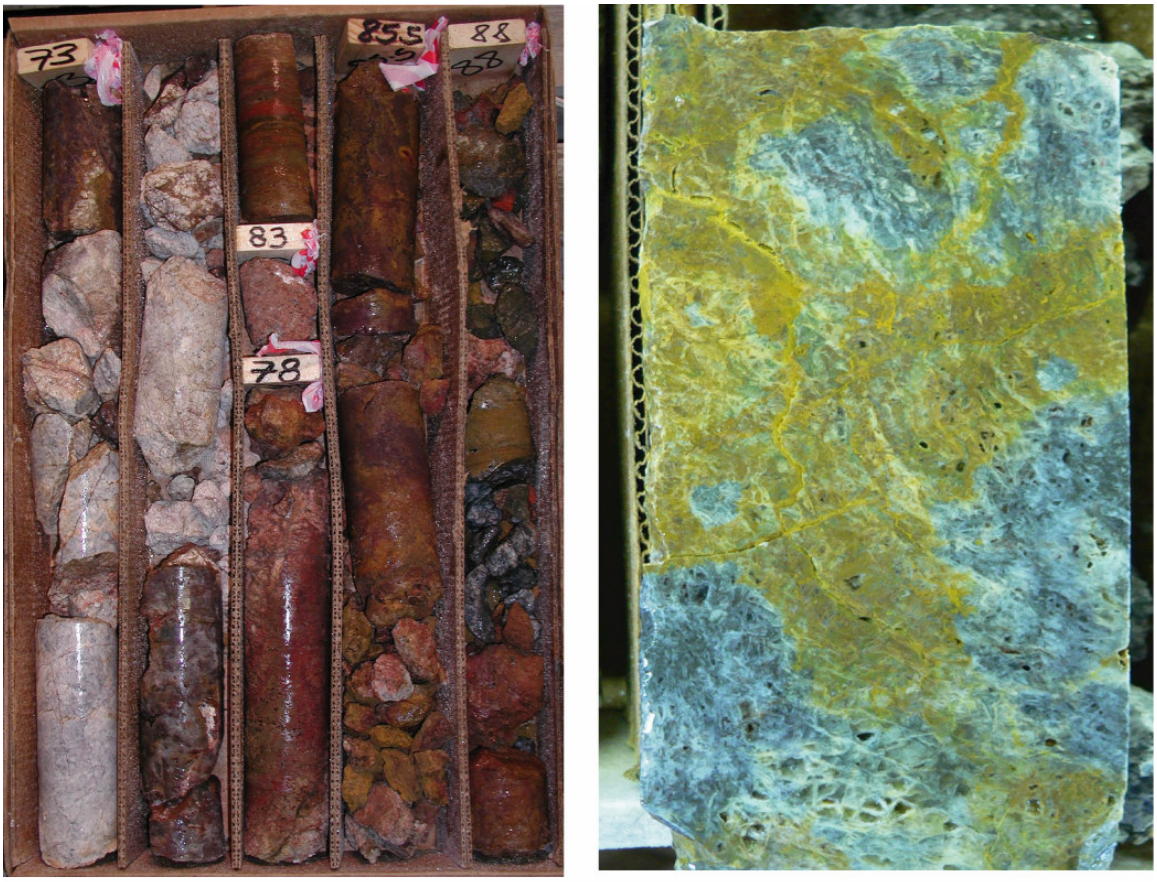

Figure 24. Intense oxidation of sulfide rich interval of core. The light pink to tan rock is weak to moderately oxidized dolomite fragments. The second photo shows iron-oxides forming along quartz-pyrite veinlets that cut an intensily silicified breccia.

Percolation of oxygen-rich meteoric water causes local oxidation of sulfides which led to the generation of acidic fluids that continue to percolate downward through the breccia bodies and along fault zones. These acidic fluids dissolve and leach the remaining carbonate material that they encounter, creating a vuggy-silica texture where the carbonate is found as fragments within silicified breccia bodies (Fig. 24). Zones of abundant hematite and local goethite are commonly seen along within the Dee fault zone.

The flow of highly acidic fluids through the Storm deposit is still an ongoing process. Before the regional water table was significantly lowered by the Goldstrike mining operations, water encountered within the Dee-Deep North deposits was reported to be in excess of 65°C (150°F) (Snyder, 1989). Even today, rock temperatures in the exploration decline can locally exceed 50°C (120°F) and steam is constantly emitted from encountered voids.

Geochemical Distributions

The mineralized zones at Storm occur as tabular bodies that are elongated in a north-northwest direction and dip shallowly to the north from the Dee open pit. They are hosted within the Dee and Ben Fault zones, respectively, and their geometries generally reflect that of the encompassing structural zones. Elemental distributions of precious metals as well as associated pathfinder elements suggest that the aerial extent of the mineralizing hydrothermal system(s) extends far beyond the Storm and Dee orebodies.

Anamolous intercepts of both gold and silver have been encountered throughout the Storm property. The majority of gold values are found within breccia bodies found along structures or igneous dike units, although low levels of anomalous gold, up to 2 grams/ton, have been found within upper plate rocks.

Outside of the main mineralized areas, silver values are encountered in lower plate rocks and are associated with structures and igneous dikes. Extremely high values, up to 1.5 kilograms/ton over 1.52 meters, have been documented in silicified upper plate rocks and suggest that the epithermal silver system is much more extensive than the Carlin gold event. Several silver occurrences occur within 10 kilometers of Storm and may represent a widespread event related to the Miocene Northern Nevada Rift epithermal mineralization. These deposits include the Ivanhoe gold-silver deposit (10 km NW; Wallace, 2003), the Rodeo Creek gold-silver occurrence (4 km NNW; Theodore et al., 2003), and the Rossi barite pit, in which Snyder (1989) recognized visible gold in thin quartz veinlets that cross-cut massive barite horizons.

Pathfinder elements commonly used for Carlin-type deposit exploration (As, Sb, Hg, and Tl) show variable zoning characteristics around the mineralized zones at Storm, yet invariably occur within the bounds of major faults. Arsenic concentrations tend to be highest with the orebodies (>500 grams/ton) and zone upwards into unmineralized breccia bodies to form a low-concentration halo. Antimony, unlike arsenic tends to be restricted to the orebodies and form a low grade halo beneath the mineralization. Thallium and mercury tend to be show elevated values only in mineralized zones.

Microthermometry

The abundance of quartz at Storm makes it a great candidate for fluid inclusion studies. Two generations of quartz, the Carlin silicification and post-Carlin veining stages, have provided enough fluid inclusion data to compare individual quartz generations (Fig. 25).

Carlin-related quartz crystals from non-jasperoided zones yielded 36 homogenization temperatures that included 8 inclusions of secondary or questionable origin. All of the analyzed inclusions were liquid dominant and range from 4 to 12 microns in diameter. The majority of inclusions were found within crystal growth zones and had no physical indications of being necked. The average temperature of primary inclusions from this stage of silicification was approximately 259.4^{o}C, with a range of 200.0 to 339.8^{o}C (Fig. 26). Other inclusions, which were suspected of being secondary in nature or were not within the field of view of other primary inclusions, were noticeably warmer, averaging 331.7^{o}C, and ranged from 186.2 to 373.3^{o} C. Although there are only limited freezing point determinations, the data suggest a low salinity fluid with less than 3.0 wt. percent NaCl equivalent. These data are in agreement with other studies that suggest a moderate temperature, low salinity fluid was responsible for the creation of most Carlin-type gold deposits, although they do represent the high end of the temperature range (Cline et al., 2005).

Post-Carlin quartz veins yielded 30 homogenization temperatures that included 4 inclusions of secondary or questionable origin. These are all liquid dominant inclusions

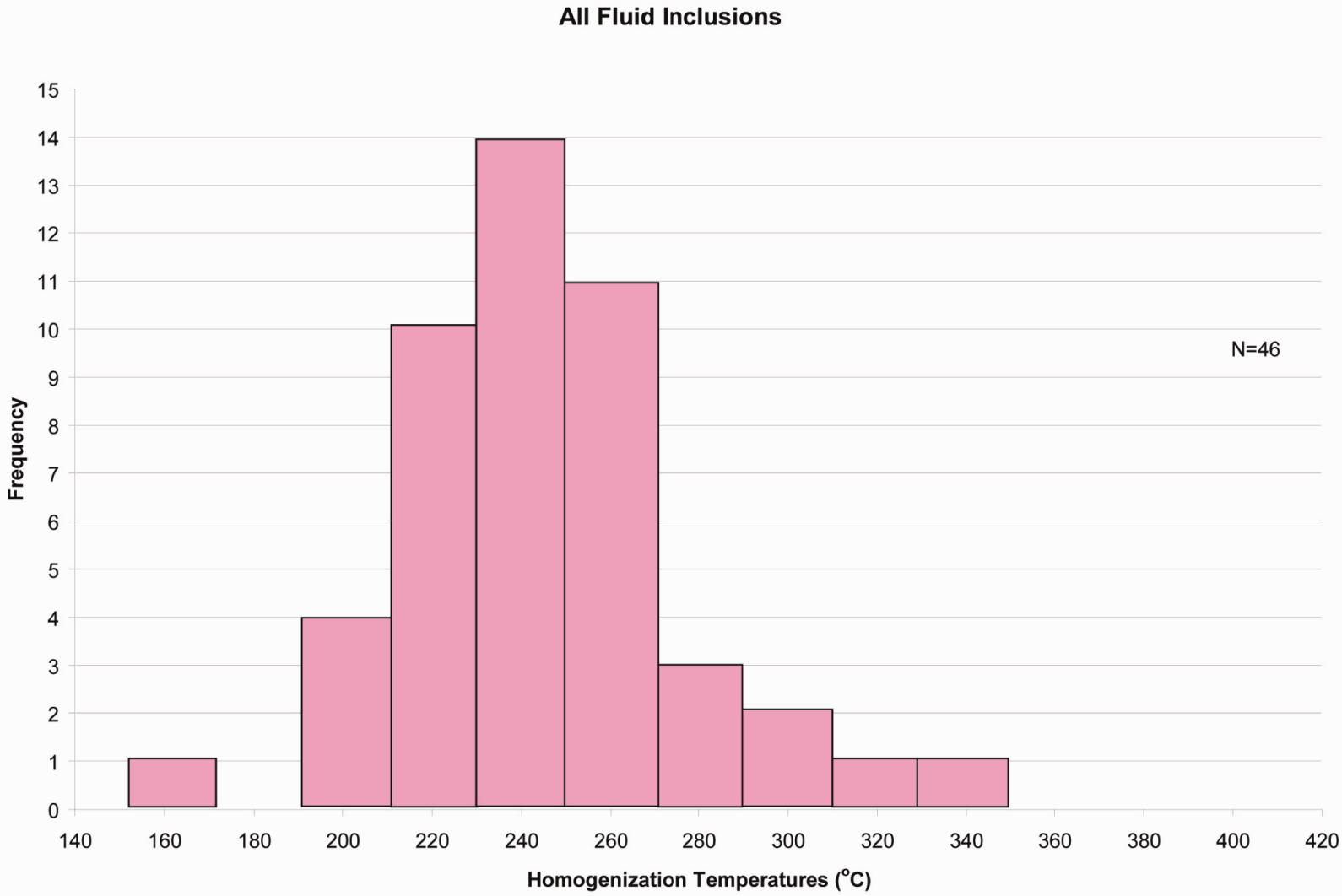

Figure 25. Histogram of fluid inclusion data from the Storm system including both Carlin and post-Carlin stage homogenization temperatures.

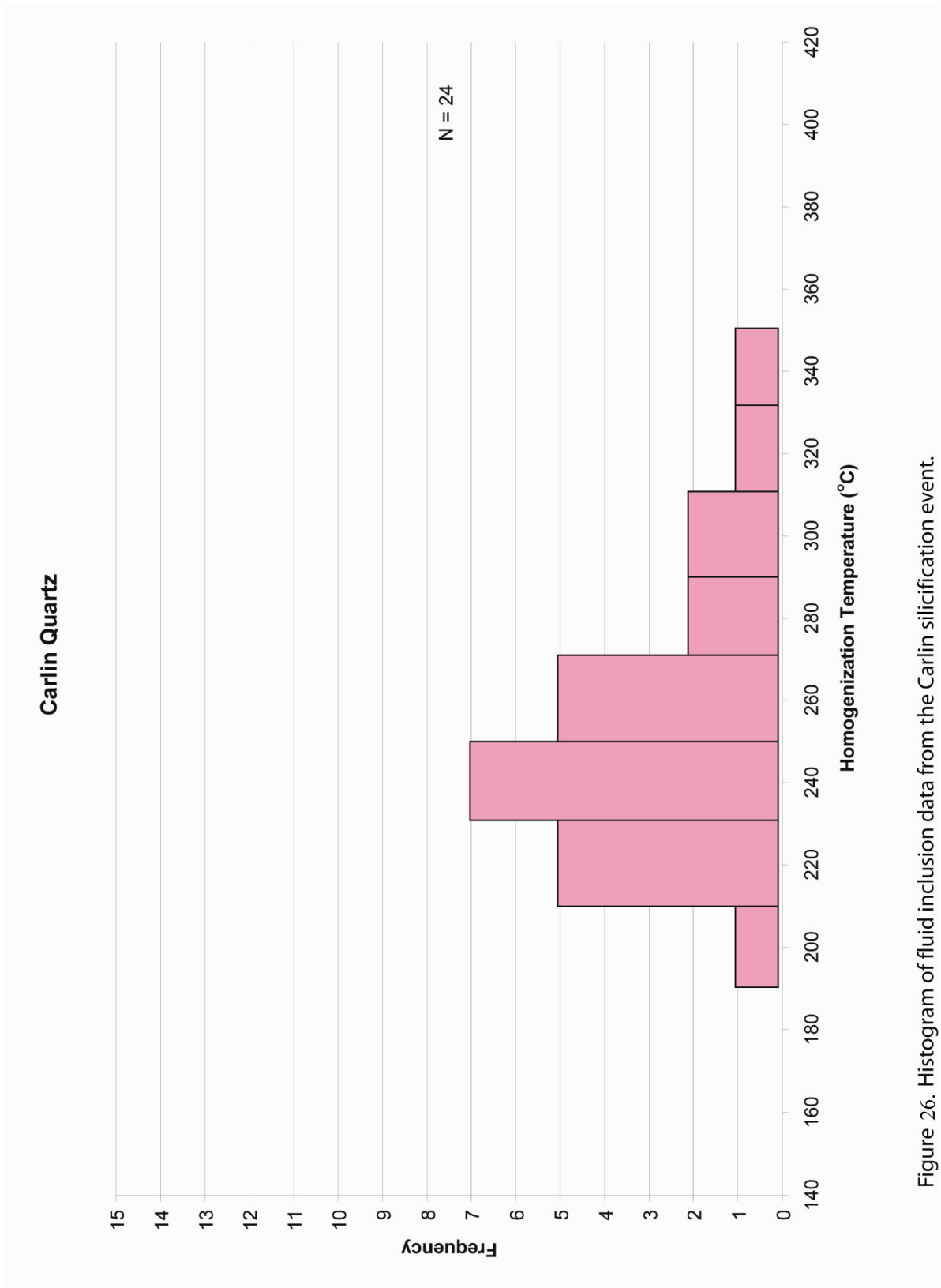

Figure 26. Histogram of fluid inclusion data from the Carlin silicification event.

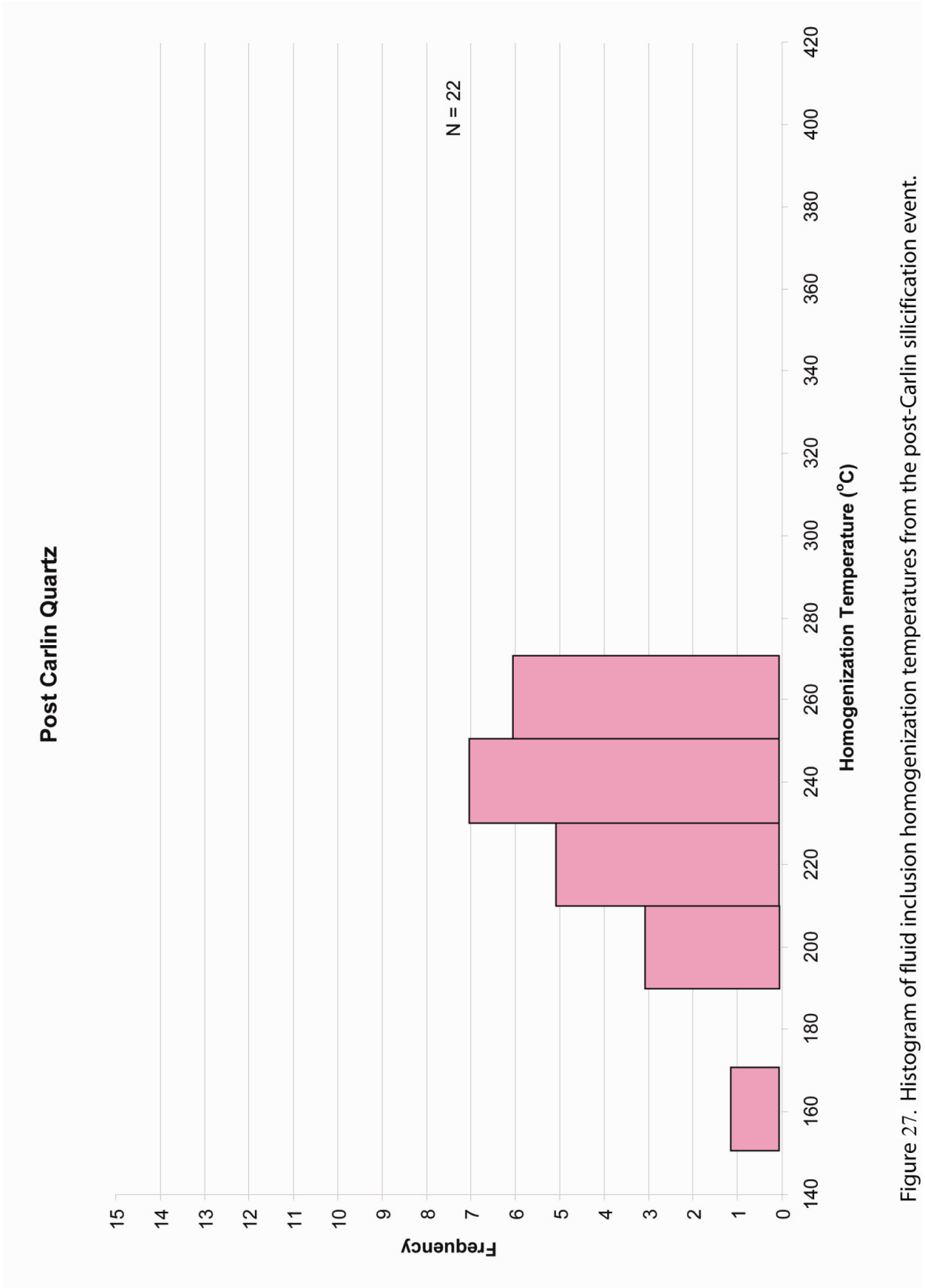

Figure 27. Histogram of fluid inclusion homogenization temperatures from the post-Carlin silicification event.

(L+V) that ranged from 5 to 20 microns in diameter. The average temperature of primary inclusions was 240.4°C, with a range of 157.5 to 312.6°C (Fig. 27). Possible secondary inclusions averaged 185.0°C and ranged from 179.6 to 212.5°C. Freezing point determinations on 3 inclusions show salinities of less than 2.0 wt. percent NaCl equivalent. The data show the hydrothermal fluids responsible for the deposition of post-Carlin quartz were cooler than the late-Carlin stage silicification. All fluid inclusion data are presented in Appendix I.

Rare fluid inclusions were identified in the main-stage jasperoid, but unfortunately the small size of the inclusions (<5 microns) and dark nature of the quartz made them too difficult to retrieve accurate data. The silver-rich quartz veins and quartz-pyrite veins yielded no usable fluid inclusions. No vapor-rich fluid inclusions were observed. Limited inclusion data on barites suggests they precipitated from a late, relatively low temperature fluid (158°C).

Apatite Fission Track Analysis

One of the early goals of this research was to try and determine whether the mineralization at Storm could be explained by a simple change in Carlin-type fluid chemistry as it evolved in time and space, or if there were actually more than one hydrothermal system responsible for the high levels of both gold and silver. To determine the relative age of the silver-rich veining event, which clearly cuts earlier Carlin mineralization, one sample of biotite-hornblende lamprophyre dike from the 49'er zone was chosen to undergo apatite fission-track (AFT) analysis. This well mineralized sample (36.7 g/t gold, 37.3 g/t silver) was selected on the basis that it contained both Carlin ore stage pyrite, post-Carlin quartz veining, and thin silver-veinlets as well as a relative abundance of visible apatite crystals included within the post-Carlin quartz crystals. The AFT analysis was meant to determine when the most recent sustained pulse of hydrothermal fluid (>105-110^{o}C) was flowing in the Storm system. The results suggest the apatite has retained fission tracks since 8 to 20 Ma (95% confidence; Duddy, 2005).

According to Duddy (2005), several explanations of this age exist and include: 1) the age reflects cooling of both the mineralized dike and surrounding host rocks due to a regional exhumation event; 2) cooling following an Early to Late Miocene hydrothermal event that sustained temperatures >105^{o}C, which may or may not be related to mineralization; and 3) the date reflects a crystallization age of the apatite. Texturally, the recovered apatite grains were euhedral crystals (80-250μ in diameter) that are mostly, if

not entirely, of hydrothermal origin. This indicates that the apatite was not an original component of the lamprophyre dike.

Due to a very low rate of exhumation in northern Nevada during the Eocene-Miocene (McGrew et al., 2000), this author is suggesting that the fission track age for the Storm deposit represents either cooling from a Miocene hydrothermal event or the crystallization age of the apatite within the quartz veins. Both could be explained by a Miocene hydrothermal event that deposited both the apatite-bearing quartz veins as well as the silver-bearing quartz veins.

Interpretations

The generation of the Storm deposit is interpreted to have occurred during six broad stages of overlapping structural preparation, hydrothermal alteration, and mineralization of both gold and silver.

Paleozoic: The first stage of development at Storm was the evolution of a structural framework that would allow access for later hydrothermal fluids. The onset of normal faulting led to the creation of a series of north to north-east striking faults that generated variable thicknesses of tectonic breccias. Further brecciation, both pre- and post-mineralization, caused local fragmentation of Jurassic dikes. The flow of early hydrothermal fluids rich in Fe, Mg, and Mn along structural zones caused the precursor limestone to be replaced by ferroan-dolomite. Alteration during this event was limited to areas within fault systems, especially within tectonic breccia bodies, as well as along favorable stratigraphic contacts that are locally intersected by such faults. Dolomitization of carbonate units resulted in volume reduction and subsequent collapse brecciation that further increased permeability and porosity throughout the system.

Mesozoic: Emplacement of lamprophyre dikes during the Jurassic both cut and locally filled the north- to northwest-striking fault-related breccia bodies. Sulfur-rich fluids related to igneous activity along the northern Carlin trend during the late Jurassic caused widespread sulfidation of ferroan-dolomite and iron-bearing silicates within the

lamprophyre dikes. The precipitation of sulfosalts and iron-bearing sphalerite are attributed to this event.

Carlin Mineralization: Auriferous fluids were channeled along faults and igneous dikes and spread out laterally along collapse breccias formed at stratigraphic contacts (particularly the Bootstrap-Popovich formations contact). These fluids generated early alteration that included decarbonatized, argillized, and sulfidized rocks. The main stage of gold deposition occurred during the Carlin event and is represented by fine-grained arsenian rims on pre-ore pyrites as well as complete replacements of pyrite grains. The concentration of silver within the main-stage gold event was up to half that of gold, with gold to silver ratios averaging ~4:1. Deposition of hypogene Au^{o} occurred contemporaneous with the arsenian pyrite.

Quartz-Veining & Jasperoids: The third stage represents the quartz veining and jasperoid event that followed Carlin mineralization. Jasperoids commonly encapsulate hypogene Au^{o}, pyrite, and arsenian gold-bearing pyrite grains. Intense quartz veining and flooding within the breccia bodies is locally associated with apatite inclusions in quartz as well as massive stibnite. This stage may represent a distinct hydrothermal event or may be closely associated with either the waning stages of the Carlin-type system or the onset of the low-sulfidation epithermal system.

Silver-Rich Veining: The evolution of a second hydrothermal system following the Carlin mineralizing event resulted in an overprinting silver-rich, low-sulfidation vein

system at Storm. Millimeter scale quartz veins cut the dense silica-sulfide breccia bodies and are locally filled by silver- and antimony-rich pyrite and selenides. A network of thin pyrite ± quartz veins are the last event related to this period of hydrothermal activity and clearly cut all younger stages of mineralization. These pyrites contain elevated concentration of antimony, yet are barren of silver.

The proximity of Storm to the Northern Nevada Rift and particularly to low sulfidation gold-silver vein deposits along it suggests a possible temporal and/or genetic association to the mid-Miocene deposits. Apatite fission track dates from Storm suggest the presence of hydrothermal fluids during this same time period (Miocene) but are unable to confirm whether those fluids were responsible for mineralization.

Pliocene Collapse Brecciation: Post-mineral collapse brecciation occurred within the 49'er and End Zone deposits and locally displaces gold and silver mineralized ore. These non- to weakly-lithified breccias formed due to the continued removal of carbonate material from the lower portions of pre-existing tectonic and collapse breccia zones. Late calcite and dolomite veining are widespread around the periphery of mineralized zones and locally flood the interstitial space within post-mineral collapse breccias. Barite is believed to be deposited at the end of the carbonate event.

Supergene: The final stage in the development of the Storm deposit is related to the supergene oxidation of the sulfides along permeable fault and fracture networks. Oxidation of both barren and mineralized sulfides generated acidic fluids that percolated

down through breccia bodies and along fault and fracture networks, dissolving any encountered carbonate material. The vuggy texture commonly seen in silicified zones resulted from the leaching of carbonate fragments from the encasing silica framework. Post-mineral calcite and dolomite veins are generally leached when oxidizing fluids are encountered.

Conclusion

The presence of both high-grade gold and silver mineralization at Storm is due to the overprinting of a Carlin-type gold system of Eocene age by a younger epithermal silver mineralizing system, of possible Miocene age, similar to those found along the Northern Nevada Rift (i.e., Midas, Ivanhoe, Mule Canyon, etc.). The juxtaposition of both ore types is a product of the Storm deposits' proximity to the Northern Nevada Rift (Miocene) and the pre-existing structural framework that provided ample space for the migration of post-Carlin hydrothermal fluids. While the concentration of silver in this system is not economic on its own, the added value of by-product silver credits will to make this deposit more profitable, especially in the period of elevated commodity prices. Exploration at the intersection of these two prolific "trends" should hopefully lead to the discovery of another overprinted system in the near future.

Appendix I. Microthermometric Data

Sample ID	Drill-Hole	Footage	Chip	Homogenization Temp	Freezing Temp	Location	Quartz-Genesis
ES43-10	ES4-040-3	131.25	5	326.30	-0.8	End Zone	Carlin
ES43-13	ES4-040-3	131.25	5	295.00	-7.4	End Zone	Carlin
ES43-1	ES4-040-3	131.25	5	235.00		End Zone	Carlin
ES43-2	ES4-040-3	131.25	5	235.30		End Zone	Carlin
ES43-3	ES4-040-3	131.25	5	235.10		End Zone	Carlin
ES43-4	ES4-040-3	131.25	5	242.70		End Zone	Carlin
ES43-5	ES4-040-3	131.25	5	186.20		End Zone	Carlin
ES43-6	ES4-040-3	131.25	5	200.00		End Zone	Carlin
ES43-7	ES4-040-3	131.25	5	206.80		End Zone	Carlin
ES43-8	ES4-040-3	131.25	5	248.80		End Zone	Carlin
ES43-9	ES4-040-3	131.25	5	247.10		End Zone	Carlin
ES43-11	ES4-040-3	131.25	5	235.10		End Zone	Carlin
ES43-12	ES4-040-3	131.25	5	231.80		End Zone	Carlin
ES43-14	ES4-040-3	131.25	5	227.10		End Zone	Carlin
ES43-15	ES4-040-3	131.25	5	338.70		End Zone	Carlin
ES43-16	ES4-040-3	131.25	5	357.80		End Zone	Carlin
ES43-17	ES4-040-3	131.25	5	315.50		End Zone	Carlin
ES43-18	ES4-040-3	131.25	5	360.00		End Zone	Carlin
ES43-19	ES4-040-3	131.25	5	357.10		End Zone	Carlin
ES43-20	ES4-040-3	131.25	5	300.20		End Zone	Carlin
ES43-21	ES4-040-3	131.25	5	258.60		End Zone	Carlin
ES43-22	ES4-040-3	131.25	5	239.50		End Zone	Carlin
ES43-23	ES4-040-3	131.25	5	291.50		End Zone	Carlin
ES43-24	ES4-040-3	131.25	5	332.40		End Zone	Carlin
ES43-25	ES4-040-3	131.25	5	274.60		End Zone	Carlin
ES43-26	ES4-040-3	131.25	5	274.50		End Zone	Carlin

ES43-27	ES4-040-3	131.25	5	339.80		End Zone	Carlin
ES43-28	ES4-040-3	131.25	5	344.50		End Zone	Carlin
ES43-29	ES4-040-3	131.25	5	243.00		End Zone	Carlin
ES43-30	ES4-040-3	131.25	5	370.20		End Zone	Carlin
ES43-31	ES4-040-3	131.25	5	373.50		End Zone	Carlin
ES43-32	ES4-040-3	131.25	5	346.90		End Zone	Carlin
ES43-33	ES4-040-3	131.25	4	210.10		End Zone	Carlin
ES43-34	ES4-040-3	131.25	4	215.90		End Zone	Carlin
ES43-35	ES4-040-3	131.25	4	210.40		End Zone	Carlin
ES43-36	ES4-040-3	131.25	4	210.70		End Zone	Carlin

Sample ID	Drill-Hole	Footage	Chip	Homogenization Temp	Freezing Temp	Location	Quartz-Genesis
R117B-1	S1-280-8	91	2	226.40		49'er Zone	Post-Carlin
R117B-2	S1-280-8	91	2	216.00		49'er Zone	Post-Carlin
R117B-3	S1-280-8	91	2	232.10		49'er Zone	Post-Carlin
R117B-4	S1-280-8	91	2	191.80		49'er Zone	Post-Carlin
R117B-5	S1-280-8	91	2	254.70		49'er Zone	Post-Carlin
R117B-6	S1-280-8	91	2	179.60		49'er Zone	Post-Carlin
R117B-7	S1-280-8	91	2	221.90		49'er Zone	Post-Carlin
R117B-8	S1-280-8	91	2	189.40		49'er Zone	Post-Carlin
R117B-9	S1-280-8	91	2	223.90		49'er Zone	Post-Carlin
R117B-10	S1-280-8	91	2	220.00		49'er Zone	Post-Carlin
R117B-11	S1-280-8	91	2	223.30		49'er Zone	Post-Carlin
R117B-12	S1-280-8	91	2	243.50		49'er Zone	Post-Carlin
R117B-14	S1-280-8	91	5	242.30		49'er Zone	Post-Carlin
R117B-15	S1-280-8	91	5	268.20	-1	49'er Zone	Post-Carlin

R117B-16	S1-280-8	91	5	245.60		49'er Zone	Post-Carlin
R117B-17	S1-280-8	91	5	192.40		49'er Zone	Post-Carlin
R117B-18	S1-280-8	91	5	253.20	-2.4	49'er Zone	Post-Carlin
R117B-19	S1-280-8	91	5	259.10		49'er Zone	Post-Carlin
R117B-20	S1-280-8	91	5	208.00		49'er Zone	Post-Carlin
R117B-21	S1-280-8	91	5	253.20	-3.2	49'er Zone	Post-Carlin
R117B-22	S1-280-8	91	5	230.50		49'er Zone	Post-Carlin
R117B-23	S1-280-8	91	5	312.60		49'er Zone	Post-Carlin
R117B-24	S1-280-8	91	5	281.30		49'er Zone	Post-Carlin
R117B-25	S1-280-8	91	5	299.80		49'er Zone	Post-Carlin
R117B-26	S1-280-8	91	5	279.90		49'er Zone	Post-Carlin
R117B-13	S1-280-8	91	5	157.50		49'er Zone	Post-Carlin
R028A-1	S1-280-2	174.6	4	218.50		49'er Zone	Post-Carlin
R028A-2	S1-280-2	174.6	4	212.50		49'er Zone	Post-Carlin
R028A-3	S1-280-2	174.6	4	237.10		49'er Zone	Post-Carlin
R028A-4	S1-280-2	174.6	4	219.30		49'er Zone	Post-Carlin

References

Arehart, G.B., Kesler, S.E., O'Neil, J.R. and Foland, K.A., 1992, Evidence for the supergene origin of alunite in sediment-hosted micron gold deposits, Nevada; Economic Geology, v. 87, p. 263-271.

Arehart, G. B., 1996, Characteristics and origin of sediment-hosted disseminated gold deposits: a review: Ore Geology Reviews, v. 11, p. 383-403.

Armstrong, A. K., Theodore, T. G., Kotlyar, B. B., Lauha, E. G., Griffin, G. L., Lorge, D. L., and Abbott, E. W., 1997, Preliminary Facies Analysis of Devonian Autochthonous Rocks that Host Gold Along the Carlin Trend, Nevada: Guidebook Series, vol. 28, p. 53-73.

Bagby, W.C., and Berger, B.R., 1985, Geologic characteristics of sediment-hosted, disseminated precious metal deposits in the western United States: Reviews in Economic Geology, v. 2, p. 169-202.

Bakken, B. M., and Einaudi, M. T., 1986, Spatial and Temporal Relations Between Wall Rock Alteration and Gold Mineralization, Main Pit, Carlin Gold Mine, Nevada, U.S.A: Gold '86; An International Symposium on the Geology of Gold Deposits; Proceedings Volume, Toronto, ON, Canada.

Bergwall, F., 1991, Geology of the Dee Gold Mine: Geologic Society of Nevada Guidebook 12, Geology and ore deposits of the Great Basin, p. 987.

Bettles, K., 2002, Exploration and Geology, 1962-2002, at the Goldstrike Property, Carlin Trend, Nevada, *in* Thompson T. B., Teal, L., and Meeuwig, R. O., eds, Gold Deposits of the Carlin Trend: Nevada Bureau of Mines and Geology, Report: 111, p. 54-75.

Castor, S.B., Boden, D.R., Henry, C.D., Cline, J.S., Hofstra, A.H., McIntosh, W.C., Tosdal, R.M., and Wooden, J.P., 2003, The Tuscarora Au-Ag District: Eocene Volcanic-Hosted Epithermal Deposits in the Carlin Gold Region, Nevada: Economic Geology, vol. 98, p. 339-366.

Cline, J. S., 2001, Timing of Gold and arsenic Sulfide Mineral Deposition at the Getchell Carlin-Type Gold Deposit, North-Central Nevada: Economic Geology, vol. 96, p. 75-89.

Cline, J. S., Hofstra, A. H., Muntean, J. L., Tosdal, R. M., and Hickey, K. A., 2005, Carlin-Type Gold Deposits in Nevada: Critical Geologic Characteristics and Viable Models, *in* Hedenquist, J. W., Thompson, J. F. H., Goldfarb, R. J., and

Richards, J. P., eds, One Hundredth Anniversary Volume: 1905-2005: Economic Geology, p. 1135.

Cook, D., Crackel, D., and Jensen, M., 2002, The Dee North Mine, Elko County, Nevada: The Mineralogical Record, vol. 33, p. 225-234.

Dobak, P.J., Arbonies, D., Hipsley, R., and Visher, M., 2002, Geology of the Storm Gold Deposit, *in* Thompson T. B., Teal, L., and Meeuwig, R. O., eds, Gold deposits of the Carlin Trend: Nevada Bureau of Mines and Geology, Bulletin 111, p. 46-53.

Dong, G., Morrison, G., and Jaireth, S., 1995, Quartz Textures in Epithermal Veins, Queensland – Classification, Origin, and Implication: Economic Geology, v. 90, p. 1841-1856.

Duddy, I. R., 2005, Apatite Fission Track Analysis (AFTA) of a Mineralised Dyke Sample from the Storm Gold Deposit, Nevada: Unpublished Geotrack Report, no. 949, 70 p.

Emsbo, P., Hofstra, A. H., Park, D., Zimmerman, J. M., and Snee, L.W., 1996, A Mid-Tertiary Age Constraint on Alteration and Mineralization in Igneous Dikes on the Goldstrike Property, Carlin Trend, Nevada: Abstracts with Programs, Geological Society of America, vol. 28, no. 7, p. 476.

Emsbo, P., 1999, Origin of the Meikle high grade gold deposit from the superposition of Late Devonian sedex and mid-Tertiary Carlin-type gold mineralization: Unpublished Ph.D. thesis, Golden, Colorado, Colorado School of Mines, 394 p.

Emsbo, P., Hofstra, A.H., and Lauha, E.A., 2000, Jurassic auriferous polymetallic mineralization at the Goldstrike mine, Carlin trend, Nevada [abs.], *in* Cluer, J.K., Price, J.G., Struhsacker, E.M., Hardyman, R.F., and Morris, C.L., eds., Geology and ore deposits 2000: The Great basin and beyond. Symposium proceedings: Reno, Geological Society of Nevada, p. 46.

Emsbo, P., and Hofstra, A.H., 2003, Origin and significance of postore dissolution collapse breccias cemented with calcite and barite at the Meikle gold deposit, northern Carlin trend, Nevada: Economic Geology, v. 98, p. 1243–1252.

Ettner, D. C., 1989, Stratigraphy and Structure of the Devonian Autochthonous Rocks, North-Central Carlin Trend of the Southern Tuscarora Mountains, Northern Eureka County, Nevada: Masters Thesis, Idaho State University, Pocatello, ID.

Evans, D. C., 2000, Carbonate-Hosted Breccias in the Meikle Mine, Nevada and Their Relationship with Gold Mineralization: Masters Thesis, Colorado School of Mines, Golden, CO.

Fleck, R. J., Theodore, T. G., Sarna-Wojcicki, A.M., and Meyer, C.E., 1998, Age and Possible Source of Air-Fall Tuffs of the Miocene Carlin Formation, Northern Nevada: U.S. Geological Survey Open-File Report: OF 98-0338-B, p. 176-192.

Furley, R., 2002, Sequence Stratigraphic Framework for the Silurian-Devonian Bootstrap Limestone, Roberts Mountains, and Devonian Popovich Formations, Northern Carlin Trend, Elko and Eureka Counties, Nevada; Unpublished Thesis, Colorado School of Mines, 208 p.

Griffin, G.L., 2000, Paleogeography of Late Silurian-Devonian autochthonous carbonates: Implications for old faults and intrusive distribution, Goldstrike property, Nevada [abs.], *in* Cluer, J.K., Price, J.G., Struhsacker, E.M., Hardyman, R.F., and Morris, C.L., eds., Geology and ore deposits 2000: The Great Basin and beyond: Reno, Geological Society of Nevada, Symposium proceedings, p. 52.

Hausen, D. M., and Kerr, P.F., 1968, Fine gold occurrence at Carlin, Nevada, *in* Ridge, J.D., ed., Ore deposits of the United States, 1933-1967: New York, American Institute of Mining Engineers, v. 1, p. 908-940.

Henkelman, C. A., 2004, Pyrite Geochemistry Across the Betze-Post Deposit, Northern Carlin Trend, Nevada; Masters Thesis, University of Nevada, Las Vegas, M.S. Thesis, 150 p.

Hitzman, M. W., 1999, Routine Staining of Drill Core to Determine Carbonate Mineralogy and Distinguish Carbonate Alteration Textures: Mineralium Deposita, v. 34, p. 794-798.

Hofstra, A. H., and Cline, J. S., 2000, Characteristics and models for Carlin-Type Gold Deposits: Reviews in Economic Geology, vol. 13, p. 163-220.

Jory, J., 2002, Stratigraphy and Host Rock Controls of Gold Deposits of the Northern Carlin Trend, *in* Thompson T. B., Teal, L., and Meeuwig, R. O., eds., Gold deposits of the Carlin Trend: Nevada Bureau of Mines and Geology, Bulletin 111, p. 20-34.

Kuehn, C.A., and Rose, A.W., 1992, Geology and Geochemistry of Wall-Rock Alteration at the Carlin Gold Deposit, Nevada: Economic Geology, vol. 87, p. 1697-1721.

Leavitt, E.D. and Arehart, G.B., 2005, Alteration, Geochemistry and Paragenesis of the Midas Epithermal Gold-Silver Deposit, Elko County, Nevada; in Rhoden, H.N., Steininger, R.C. and Vikre, P.G., editors, *Geological Society of Nevada Symposium 2005: Window to the World*, p. 563-627.

Leavitt, E.D., Spell, T.L, Wallace, A.R., Goldstrand, P.M., and Arehart, G.B., 2004, Geochronology of the Midas low-sulfidation epithermal gold-silver deposit, Elko County, Nevada; *Economic Geology*, v. 99, p. 1665-1686.

Leonardson, R.W., and Rahn, J.E., 1996, Geology of the Betze-Post gold deposits, Eureka County, Nevada, *in* Coyner, A.R., and Fahey, P.L., eds., Geology and ore deposits of the American Cordillera: Geological Society of Nevada, Reno, Nevada. P. 61-94.

Lubben, J., 2004, Silicification Across the Betze-Post Carlin-type Au Deposit: Clues to Ore Fluid Properties and Sources, Northern Carlin Trend, Nevada; Masters Thesis, University of Nevada, Las Vegas, p. 155.

McCrea, J.M., 1950, On the Isotope Chemistry of Carbonates and a Paleotemperature Scale: Journal of Chemical Physics, vol. 18: p. 849-857.

McGrew, A. J., Peters, M. T. & Wright, J. E. (2000). Thermobarometric constraints on the tectonothermal evolution of the East Humboldt Range metamorphic core complex, Nevada. *Geological Society of America Bulletin* 112, 45–60

Nuckolls, H. M., 1985, Geology of the Bootstrap Mine, Nevada; A Sediment-Hosted Disseminated Gold Deposit: Masters Thesis, Stanford University, Stanford, CA.

Ressel, M. W., Noble, D. C., Henry, C. D., and Trudel, W. S., 2000, Dike-Hosted ores of the Beast Deposit and the importance of Eocene Magmatic in Gold Mineralization of the Carlin Trend, Nevada: Economic Geology and the Bulletin of the Society of Economic Geologists, vol. 95, no. 7, p. 1417-1444.

Radtke, S., Heropoulos, C., Fabbi, B.P., Scheiner, B.J., and Essington, M., 1972, Data on Major and Minor Elements in Host Rocks and Ores, Carlin Gold Deposit, Nevada: Economic Geology, v. 67, n. 2, p. 975-978.

Ressel, M. W., 2000, Summary of Research on Igneous Rocks and Gold Deposits of the Carlin Trend, Nevada: Ralph J. Roberts Center for Research in Economic Geology Annual Research Meeting – 1999, Program and Reports, 38 p.

Ressel, M.W., and Henry, C.D., 2006, Igneous geology of the Carlin trend, Nevada: Development of the Eocene plutonic complex and significance for Carlin-type gold deposits: Economic Geology, v. 101, p. 347-383.

Ressel, M.W., 2005, Igneous geology of the Carlin trend, Nevada: The importance of Eocene magmatism in gold mineralization, unpublished dissertation, University of Nevada, Reno, 276 p.

Roberts, R. J., 1960, Paleozoic Structure in the Great Basin: Geological Society of America Bulletin, vol. 71, no. 12, part 2, p. 1955.

Simon, G., Kesler, S.E., and Chryssoulis, S., 1999, Geochemistry and Textures of Gold-Bearing Arsenian Pyrite, Twin Creeks, Nevada: Implications for Deposition of Gold in Carlin-Type Deposits: Economic Geology, vol. 94, p. 405-421.

Snyder, K. D., 1989, Geology and Mineral Deposits of the Rossi Mine area, Elko County, Nevada: Doctoral Dissertation, University of Nevada Reno.

Stewart, John H., 1980, Geology of Nevada: Nevada Bureau of Mines and Geology Special Publication 4, 136p.

Teal, L., and Jackson, M., 1997, Geologic overview of the Carlin trend gold deposits and descriptions of recent deep discoveries: SEG Newsletter #31, p. 1, p. 13-25.

Teal, L., and Jackson, M., 2002, Geologic Overview of the Carlin Trend gold deposits, *in* Thompson T. B., Teal, L., and Meeuwig, R. O., eds., Gold deposits of the Carlin Trend: Nevada Bureau of Mines and Geology, Bulletin 111, p. 9-19.

Theodore, T. G., Kotlyar, B. B., Singer, D. A., Berger, V. I., Abbott, E. W., and Foster, A. L., 2003, Applied Geochemistry, Geology, and Mineralogy of the Northernmost Carlin Trend, Nevada: Economic Geology, vol. 98, 2003, p. 287-316.

Thompson T. B., Teal, L., and Meeuwig, R. O., eds., Gold deposits of the Carlin Trend: Nevada Bureau of Mines and Geology, Bulletin 111, p. 20-34.

Thorman, C. H., Ketner, K. B., Brooks, W. E., and Peterson, F., 1992, The Elko Orogeny in Northeastern Nevada: Structural Geology and Petroleum Potential of Southwest Elko County, Nevada; The Guidbook to the Nevada Petroleum Society Annual Field Trip.

Wallace, A. B., 2003, Geology of the Ivanhoe Hg-Au District, Northern Nevada: Influence of Miocene Volcanism, Lakes, and Active Faulting on Epithermal Mineralization: Economic Geology, vol. 98, p. 409-424.

Wells, J., and Mullens, T., 1973, Gold-Bearing Arsenian Pyrite Determined by Microprobe Analysis, Cortez and Carlin Gold Mines, Nevada: Economic Geology, v. 68, p. 187-201.

Williams, C. L., Thompson, T. B., Powell, J. L., and Dunbar, W. W., 2000, Gold-Bearing Breccias of the Rain Mine, Carlin Trend, Nevada: Economic Geology, v. 95, p. 391-404.